Thesis for the degree of Doctor of Philosophy

Facile fabrication of stimuli-responsive biopolymeric-derived hydrogels through click chemistry for drug delivery application

by

Ali Rizwan

Department of Smart Green Technology Engineering

The Graduate School

Pukyong National University

February 2024

Facile fabrication of stimuli-responsive biopolymeric-derived hydrogels through click chemistry for drug delivery application

(약물 전달 응용을 위한 클릭 화학을 통한 자극 반응형 생체고분자 유래 하이드로겔의 손쉬운 제작)

Advisor: Prof. Kwon Taek Lim

by

Ali Rizwan

A thesis of submitted in partial fulfillment of the requirements

for the degree of

Doctor of Philosophy

in Department of Smart Green Technology Engineering, The Graduate School,

Pukyong National University

February 2024

Facile fabrication of stimuli-responsive biopolymeric-derived hydrogels through click chemistry for drug delivery application

A dissertation

by

Ali Rizwan

Approved by:

(Chairman): Prof. Kwon-Taek Lim

(Member): Prof. Bonggi Lee

(Member): Prof. Sang-Hyug Park

(Member): Prof. Yeong-Soon Gal

(Member): Prof. Yong Hyun Kim

February 16th, 2024

ACKNOWLEDGEMENT

All praises are for **ALMIGHTY ALLAH**. Countless thanks to the Lord of lords, Creator of unlimited worlds, who blessed me with zeal and zest to seek knowledge and enabled me to overcome all the difficulties.

One of the constituents of the apex of my thought-provoking process is the study of the universe and the creatures. Inspiration always arouses some question in a mind and the answer, as far as my finite knowledge is concerned, lies in the divine message ordained by the Creator and THE LORD OF WORLDS, compiled as the **HOLY QURAN**. The explication, extraction, or induction of facts from this Divine Message has a prodigious Supremacy over all the scientifically discovered from the pre-history era to the modern era, as they scientifically and logically proved even.

It is a matter of great pleasure for me to have a chance to pay my heartiest gratitude to all of those who, without any worldly benefit, endeavor to contribute to the cause of positive assignments and tasks. Firstly I express my deep sense of gratitude to MERITORIOUS **Prof. Kwon Taek Lim** who devised the research opportunities, educational facilities, technical guidance, creative writing style, and positive thinking among the students: especially in me.

With a deep emotion of gratitude, I am gratified by the unbound assistance of our collaborative research group (LATTE) **Prof. Sang Hyug Park** Department of Biomedical Engineering, Pukyong National University for his support, pieces of advice, skilled guidance, valuable comments, encouraging attitude, suggestions and provisions that benefit me much in the pursuit of studies and completion of this doctorate research thesis. Sharing his knowledge helped me in the analysis of data and its statistical computations.

I acknowledge the respective cooperation of Dr. Gulfam, Israr Ali, Sung Han Jo, and Vu Trung Thang, and express my thanks to all of them.

Ali Rizwan

Contents

List of Figures

List of Tables

List of Schemes

List of Equations

Facile fabrication of stimuli-responsive biopolymeric-derived hydrogels through click chemistry for drug delivery application

Ali Rizwan

Department of Smart Green Technology Engineering, The Graduate School
Pukyong National University

Abstract

Cross-linked bio-polymeric-derived hydrogels have been extensively studied in the development of drug delivery systems with high efficiency. The drug delivery performance of bio-polymers in transporting drug molecules within physiological conditions can be controlled through the systematic design of cross-linker chemical structures and the conjugation of bio-polymers with appropriate moieties.

In this dissertation, NIR/reduction-responsive drug delivery systems were developed by employing novel crosslinked gelatin/carboxymethyl cellulose (CMC)/Alginate (Alg)-based hydrogels. The study covers a systematic investigation of the effects of near-infrared (NIR)/reducing environment on gelatin-modified norbornene crosslinked through water-soluble diselenide di-polyethylene glycol-di-tetrazine (DSe-DPEG-DTz), cross-linker loaded with doxorubicin along with indocyanine green. Furthermore, the facile fabrication

of CMC/Alg via IEDDA click chemistry loaded with indocyanine green for photothermal and photodynamic anti-tumor therapy was also explored.

The covalent bond between polymer backbones and the cross-linkers proceeded via a "click chemistry" reaction, such as inverse electron demand diels alder (IEDDA). This type of reaction was selected owing to its simple and facile process. Biocompatibility was considered in selecting a polymer such as gelatin, CMC, and Alg. In the first study, gelatin-modified norbornene (Gel-Nb) was cross-linked with DSe-DPEG-DTz through IEDDA click chemistry to investigate the NIR/reduction-responsive behavior of the fabricated hydrogels. The release of drug (Doxorubicin) molecules could be effectively controlled by employing NIR light and reducing the environment. The second study investigated the NIR-responsive performance through CMC/Alg-derived, ICG-loaded, hydrogels fabricated through a click chemistry mechanism. NIR light (808 nm) is safe and considered a non-invasive technique for photothermal/photodynamic (PTT/PDT) anti-tumor applications.

Various analyses and characterization techniques were used in this dissertation such as proton nuclear magnetic resonance (1H-NMR) spectroscopy, Fourier transform infrared (FT-IR) spectroscopy, ultraviolet-visible (UV-vis) spectroscopy, fluorescence spectroscopy, Field emission scanning electron microscopy (FE-SEM), rheological analyses, swelling, in-vitro drug release, and anti-tumor activities.

In conclusion, the studies demonstrated that preparing a biopolymer-based drug delivery hydrogel matrix with a suitable cross-linker played a vital role. NIR and reduction-responsive hydrogels were successfully fabricated by using an IEDDA click reaction between norbornene and tetrazine moieties. The viscoelastic and morphological properties of hydrogels were greatly influenced by the concentration of the respective cross-linking molecules.

Gel-Nb was efficiently cross-linked with DSe-DPEG-DTz, resulting in a porous structure and effective mechanical properties. The DOX/ICG-loaded hydrogels released minimal amounts (26%) of DOX and (23%) of ICG at a physiological condition (PBS, pH 7.4), respectively. On the contrary, a fast release of DOX (>95%) and ICG (>80%) was observed in a reducing environment and under NIR irradiation simultaneously after 48 and 24 h respectively. The DOX/DOX+ICG-loaded hydrogels showed good efficacy under a reducing/NIR environment against BT-20 cells. The hydrogels derived from CMC/Alg exhibited viscoelastic properties (G′ ~ 492-270 Pa) and high porosity and showed a PTT/PDT anti-tumor effect. The ICG-encapsulated hydrogels demonstrated ROS generation ability under NIR exposure. The ROS production was investigated through DPBF assays to access the photodynamic effect (with NIR irradiation at 1-2W for 5-15 min). The temperature of the ICG-loaded hydrogels was also raised upon the NIR irradiation to eradicate tumor cells photothermally. The In vitro cytocompatibility assessments revealed the non-toxic nature of CMC-Nb and Alg-mTz towards HEK-293 cells. Furthermore, the ICG-loaded hydrogels effectively inhibited the metabolic activity of Hela cells following NIR exposure. This innovative hydrogel system holds promise for applications in combined PTT and PDT.

약물 전달 응용을 위한 클릭 화학을 통한 자극 반응형 생체고분자 유래 하이드로겔의 손쉬운 제작

Ali Rizwan

부경대학교 대학원 스마트그린기술융합공학과

가교된 천연 고분자 유래 하이드로겔은 고효율의 약물 전달 시스템 개발을 위해 광범위하게 연구되어 왔습니다. 생리적 조건 내에서 약물 분자를 운반하는 천연 고분자의 약물 전달 성능은 가교제 화학 구조의 체계적인 설계와 천연 고분자와 적절한 모티어와의 접합을 통해 제어할 수 있습니다.

이 논문에서는 새로운 가교 젤라틴/카복시메틸 셀룰로오스(CMC)/알지네이트(Alg) 기반 하이드로젤을 사용하여 근적외선/환원 반응성 약물 전달 시스템을 개발했습니다. 이 연구는 인도시아닌(ICG) 그린과 함께 독소루비신이 탑재된 가교제인 수용성 디셀레나이드 디 폴리에틸렌 글리콜-디 테트라진(DSe-DPEG-DTz)을 통해 가교된 젤라틴 변성 노르보넨에 대한 근적외선(NIR)/환원 환경의

영향을 체계적으로 조사했습니다. 또한, 광열 및 광역학 항암 치료를 위해 인도시아닌 그린(ICG)이 탑재된 inverse electron demand Diels-Alder (IEDDA) 클릭 화학을 통해 CMC/Alg 를 쉽게 제조할 수 있는 방법도 연구했습니다.

고분자 구조체와 가교제 사이의 공유 결합은 IEDD 와 같은 '클릭 화학 (click-chemistry)' 반응을 통해 진행되었습니다. 이러한 유형의 반응은 공정이 간단하고 쉽기 때문에 선택되었습니다.

젤라틴, CMC, Alg 와 같은 재료를 선택할 때 생체 적합성을 고려했습니다. 첫 번째 연구에서는 젤라틴 변성 노르보르넨(gelatin-norbornene, Gel-Nb)을 IEDDA 클릭 화학을 통해 DSe-DPEG-DTz 와 가교 결합하여 제조된 하이드로젤의 근적외선/환원 반응 거동을 조사했습니다. 약물(DOX) 분자의 방출은 근적외선과 환원 환경을 이용하여 효과적으로 제어할 수 있었습니다. 두 번째 연구는 클릭 화학 메커니즘을 통해 제조된 CMC/Alg 유래, ICG 탑재 하이드로젤을 통해 NIR 반응 성능을 조사했습니다. 근적외선(808nm)은 안전하며 광열/광역학(PTT/PDT) 항종양 애플리케이션을 위한 비침습적 기술로 간주됩니다.

본 논문에서는 양성자 핵자기공명(1H-NMR) 분광법, 푸리에 변환 적외선(FT-IR) 분광법, 자외선 가시광선(UV-vis) 분광법, 형광 분광법, 전계

방출 주사 전자 현미경(FE-SEM), 유변학 분석, 팽창, 체외 약물 방출 및 항종양 활성 등 다양한 분석 및 특성화 기법이 사용되었습니다.

결론적으로, 이 연구는 적절한 가교제로 생체 고분자 기반 약물 전달 하이드로겔 매트릭스를 준비하는 것이 중요한 역할을 한다는 것을 입증했습니다. 또한 근적외선 및 환원 반응성 하이드로겔은 노르보르넨과 테트라진 간의 IEDDA 클릭 반응을 사용하여 성공적으로 제조되었습니다. 하이드로겔의 점탄성 및 형태학적 특성은 각 가교 분자의 농도에 따라 크게 영향을 받았습니다.

Gel-Nb 는 DSe-DPEG-DTz 와 효율적으로 가교 결합되어 다공성 구조와 효과적인 기계적 특성을 갖게 되었습니다. DOX/ICG 가 탑재된 하이드로겔은 생리적 조건(PBS, pH 7.4)에서 각각 최소한의 DOX(26%)와 ICG(23%)를 방출했습니다. 반면, 환원 환경과 근적외선 조사에서는 각각 48 시간과 24 시간 후에 DOX(>95%)와 ICG(>80%)가 동시에 빠르게 방출되는 것이 관찰되었습니다. DOX/DOX+ICG 탑재 하이드로젤은 유방암 세포(BT-20)에 대한 환원/NIR 환경에서 우수한 효능을 보였습니다. CMC/Alg 에서 추출한 하이드로젤은 점탄성($G' \sim 492\text{-}270$ Pa)과 높은 다공성을 보였으며 PTT/PDT 항종양 효과를 나타냈습니다. ICG 캡슐화 하이드로젤은 근적외선 노출 시 ROS 생성 능력을 보여주었습니다. 광

역학 효과에 접근하기 위해 DPBF 분석을 통해 ROS 생성을 조사했습니다(1-2W, 5-15 분 NIR 조사). 또한 종양 세포를 광열적으로 박멸하기 위해 NIR 조사 시 ICG 가 탑재된 하이드로젤의 온도를 높였습니다. 시험관 내 세포 적합성 평가 결과, HEK-293 세포에 대한 CMC-Nb 및 Alg-mTz 의 무독성 특성이 밝혀졌습니다. 또한 ICG 가 탑재된 하이드로젤은 근적외선 노출 후 암세포의 대사 활동을 효과적으로 억제했습니다. 결과적으로 이러한 혁신적인 하이드로겔 시스템은 PTT 와 PDT 를 결합한 응용 분야에 대한 가능성을 제시합니다.

List of Abbreviations

CMC	Carboxymethyl cellulose
CMC-Nb	Carboxymethyl cellulose norbornene
Alg	Alginate
Alg-mTz	Alginate methyl tetrazine
DC	Drug content
DDS	Drug delivery system
DI	Deionized
DMAP	Dimethylaminopyridine
DMEM	Dulbecco's Modified Eagle Medium
DOX.HCl	Doxorubicin Hydrochloride
DS	Degree of Substitution
DSe-DPEG-DTz	diselenide-di polyethylene glycol-di tetrazine
EDC. HCl	1-ethyl-3-(3-dimethylaminopropyl)-carbodiimide hydrochloride
FBS	Fetal bovine serum
G′	Shear Storage modulus
G″	Shear Loss modulus
GSH	Glutathione
ICG	Indocyanine green
IEDDA	Inverse electron demand Diels-Alder
LVR	Linear viscoelastic region
$NaBH_4$	Sodium borohydride
Nb-NH_2	5-norbornene-2-methylamine
NHS	N-hydroxysuccinamide

NIR	Near Infrared
PEG	Polyethylene glycol
PTT	Photothermal therapy
ROS	Reactive Oxygen Species
TEA	Triethylamine
Tz	Tetrazine
γ_c	Critical strain
DEE	Drug encapsulation efficiency
FDA	Food and Drug Administration
DLE	Drug loading efficiency
MWCO	Molecular weight cut-off
DPBF	1,3-diphenylisobenzofuran

Chapter 1: Facile fabrication of stimuli-responsive biopolymeric-derived hydrogels through click chemistry for drug delivery application

1.1. Introduction

1.1.1. Background on biopolymer-derived hydrogels

Biopolymer-derived hydrogels represent a fascinating class of materials with diverse applications in fields such as biomedicine [1], tissue engineering [2], and environmental science [3]. These hydrogels are primarily composed of biopolymers, which are natural polymers derived from living organisms, such as proteins, polysaccharides, and nucleic acids. One of the key advantages of biopolymer-derived hydrogels is their biocompatibility, which makes them an excellent choice for various biomedical applications. Biopolymer-derived hydrogels offer several advantages, including biodegradability [4], biocompatibility [5], and tunable mechanical properties [4]. The nature of biopolymer-based hydrogels also allows for tailored mechanical and chemical properties, enabling them to mimic the natural extracellular matrix, which is crucial for cellular adhesion, growth, and differentiation. Researchers can modify the properties of these hydrogels to match specific requirements, such as the ability to release drugs or to support cell growth. For instance, they can be used as scaffolds for tissue regeneration [6], drug delivery systems [7], and wound dressings [8].

These hydrogels are typically created through a process known as cross-linking, where the biopolymers' molecular chains are interconnected, resulting in a three-dimensional network structure. The cross-linking can be achieved through physical, chemical, or enzymatic methods, offering flexibility in design and

customization. Furthermore, the biodegradability of many biopolymers used in these hydrogels ensures they do not persist in the environment, making them eco-friendly and sustainable. As research in biopolymer-derived hydrogels continues to advance, their potential applications expand, including water purification, food packaging, and even as eco-friendly alternatives to traditional plastics. These versatile materials hold promise in addressing various challenges and are a testament to the intersection of biology and materials science in the pursuit of sustainable and innovative solutions.

1.1.2. Significance of stimuli responsive hydrogels

Stimuli-responsive hydrogels have emerged as a remarkable class of materials with profound significance in various scientific and technological fields. These hydrogels, which exhibit dynamic changes in their physical or chemical properties in response to specific stimuli such as temperature [9], pH [10], or external stimuli such as NIR [11], hold immense promise for applications in drug delivery, tissue engineering, other biomedical fields as presented in Fig. 1. The ability of stimuli responsive hydrogels to undergo transformations allows precise control over their structure and nature of the polymer. This makes them potential candidate for targeted and controlled drug release in specific conditions. In the field of tissue engineering, stimuli-responsive hydrogels mimic the dynamic nature of extracellular matrix [12], facilitating cell growth and tissue regeneration. Furthermore, the methodologies for crafting stimuli-responsive hydrogels has brought novel concepts for controlled and targeted drug release. Overall, the significance of stimuli-responsive hydrogels lies in their versatility and adaptability, offering innovative solutions in biomedical and material science domains.

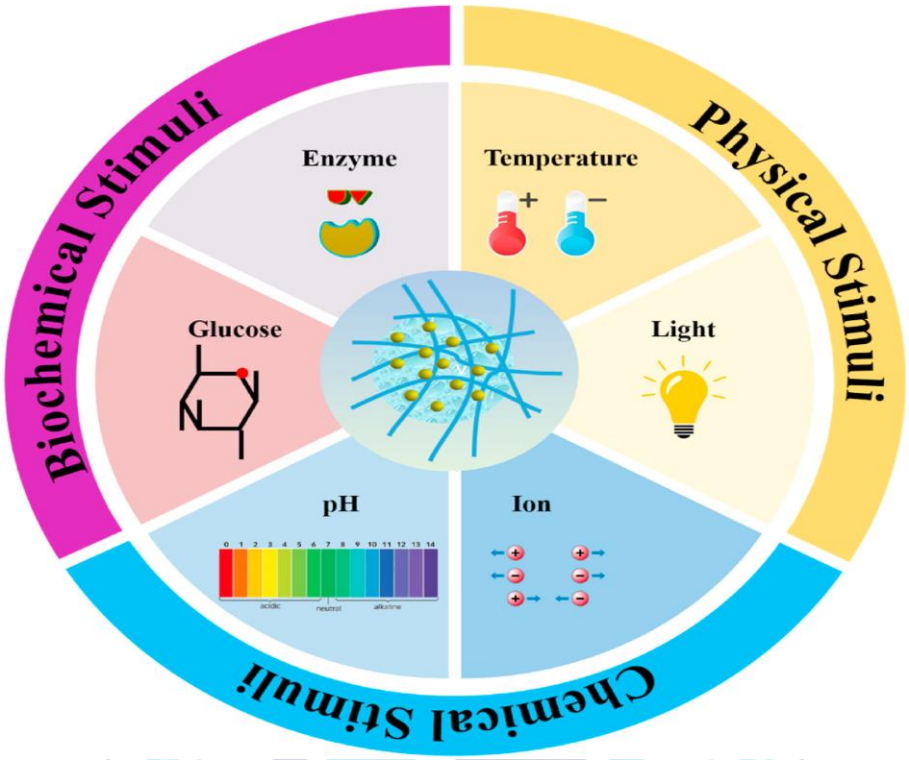

Fig. 1 classification of stimulus-responsive hydrogels

1.1.3. Use of click chemistry as a tool for hydrogel fabrication

There are various strategies to develop a hydrogel system for drug delivery applications. Some of them are physically cross-linked with less mechanical properties and poor stability leading in-efficient drug loading in such hydrogels [13], however chemically cross-linked hydrogels have tremendous advantages due to their robust mechanical properties and higher stability against degradation [14]. Due to these factors, the chemically cross-linked hydrogels are considered to be the most useful candidate for drug delivery applications. There are various strategies for developing chemically cross-linked hydrogels such as thiol-ene [15], copper click chemistry [16], diels-alder reaction (DA) [17], and Schiff-base reaction [18]. Among these chemical methodologies, inverse electron-demand Diels-Alder (IEDDA) click reaction is most suitable pathway for developing hydrogel system due to absence of any catalyst/side-product [19]. A lot of attention has been given by researchers in click chemistry to design hydrogels with tailored characteristics, such as tunable mechanical strength, biocompatibility, and responsiveness to environmental stimuli. The click chemistry-based hydrogel fabrication not only simplifies the synthesis process but also opens avenues for the development of advanced biomaterials for drug delivery, tissue engineering, and other biomedical applications. Overall, the strategic incorporation of click chemistry into hydrogel fabrication showcases its potential as a valuable tool in the quest for innovative and customizable biomaterials.

Chapter 2: Gelatin-based NIR and reduction-responsive injectable hydrogels cross-linked through IEDDA click chemistry for drug delivery application

2.1. Introduction

Stimuli-responsive hydrogels are one of the important class of polymeric materials, which can efficiently and smartly respond to various environmental stimuli including temperature, pH, ultraviolet (UV) light [9,20], redox potential [21], and near infrared (NIR) light [22]. They have been widely used in agriculture [23], sensing devices [24], biological applications [25], and drug delivery [26].The existence of various functional groups, such as amine, carboxylic acid, and sulfonic acid largely affected the physical and chemical properties of stimuli-responsive polymers [27]. Among stimuli-responsive materials, reduction [28] and NIR-responsive [29] scaffolds have gained much attention in the field of drug delivery during past years. Specifically, a substantial amount of study has been accomplished to develop hydrogels with NIR-responsive properties [30]. NIR has an advantage over other external light sources of short wavelength such as UV light which causes damage to tissues. NIR has deep penetration ability with nominal damage as compared to UV light [31]. To formulate NIR-responsive hydrogels, indocyanine green (ICG), a safe photosensitizer, is often used. ICG is used as a medical imaging agent and has the potential to produce reactive oxygen species (ROS) by absorption of NIR irradiation (808 nm) [32]. ROS can cleave weak covalent bonds, typically diselenide (Se-Se) bonds with low bond dissociation energy (172 KJ/mol) [33]. Alongside the NIR-responsive behavior of hydrogels, an extensive research has been carried out to fabricate hydrogels with redox-sensitive properties [34]. In general, the reduction-responsive scaffolds are formed by the assimilation of

disulfide and diselenide bonds into polymers. The diselenide bonds are more susceptible in a reducing environment due to the lower bonding energy, which ultimately causes the quick release of encapsulated therapeutic agents [29]. Hence, a fast reduction-responsive biomaterial could be fabricated by using diselenide bonds. However, most of diselenide-based cross-linkers cited in the literature lacked water solubility, requiring the use of hazardous solvents [35], which could compromise the biocompatibility of these systems [35]. Therefore, diselenide-based cross-linkers with good hydrophilicity and biocompatibility are in high demand for the preparation of hydrogels.

There are various biomolecules used in the preparation of intelligent hydrogels. Among them, gelatin is an enticing biomolecule derived from the partial hydrolysis of collagen found in animals. The gelatin is biodegradable [36], biocompatible [37], and has been extensively used for the fabrication of hydrogels. There are various functional groups available in the gelatin backbone, such as–COOH, $–NH_2$, and –OH groups, which enable fast physical/ionic cross-linking, making gelatin a promising candidate for hydrogel-based drug carriers [38]. However, physically cross-linked hydrogels show weak mechanical strength and poor drug encapsulation efficiency, which limits its applications in drug delivery [39]. Therefore, covalent cross-linking strategies proved to improve the durability of gelatin-based hydrogels [40].

There are various approaches for the preparation of chemically cross-linked gelatin hydrogels, such as the thiol-ene Michael-type reaction [41], azide-alkyne cycloaddition reaction [42], and photochemical cross-linking reaction [43]. Although, these methodologies are facile and convenient for the fabrication of hydrogels, most of them use toxic chemicals and catalysts, rendering them less biocompatible. Therefore, there is a need for a strategy to make gelatin-based hydrogels with minimum harmful effects. In recent times, click reactions have

gained much attention in the design of hydrogel scaffolds, leaving fewer toxic effects. Particularly, the inverse electron demand Diels-Alder (IEDDA) reaction between norbornene (Nb) groups and tetrazine (Tz) groups has been studied as an attractive "click" reaction [35]. The click IEDDA reaction provides greater chemo-selectivity with robust reaction kinetics at optimum conditions. Furthermore, it generates N_2 gas, a side product, which could be helpful for the formation of pores in the hydrogel networks [44]. The porous architecture of hydrogels can lead to achieve suitable swelling equilibrium and increase drug loading efficiency.

In the present work, we fabricated dual-stimuli (NIR and reduction) responsive and injectable gelatin hydrogels by using hydrophilic diselenide-based cross-linkers via IEDDA click reaction. As shown in Scheme 1, the synthesized cross-linker bore Tz-functional groups at its both terminals, which reacted with Nb-functionalized gelatin (Gel-Nb) to produce bioorthogonal hydrogel networks. Doxorubicin (DOX), as a standard drug, was loaded during the fabrication of gelatin-based hydrogels with >90% drug loading efficiency. In a similar test, ICG was also encapsulated with DOX in the Gel-Nb solution to formulate NIR-responsive hydrogels. When NIR light was applied, the ICG molecule produced ROS causing the breakage of diselenide bonds in the hydrogels. Consequently, a quick release of encapsulated drug occurred. The drug release studies showed minimal DOX release (30%) under physiological conditions. By contrast, a fast and continuous drug release was noticed when gelatin hydrogels were subjected to a reduction (10mM GSH) environment and/or exposed to NIR irradiation. In the examined cell line, Gel-Nb, hydrogels, and the cross-linker did not show any cytotoxicity. Meanwhile, DOX encapsulated hydrogels exhibited anti-cancer ability against breast cancer (BT-20) cell line. Similar to free-DOX and DOX

loaded hydrogels, DOX and ICGco-loaded hydrogels suppressed the proliferation of BT-20 cancer cells after the exposure to the NIR light.

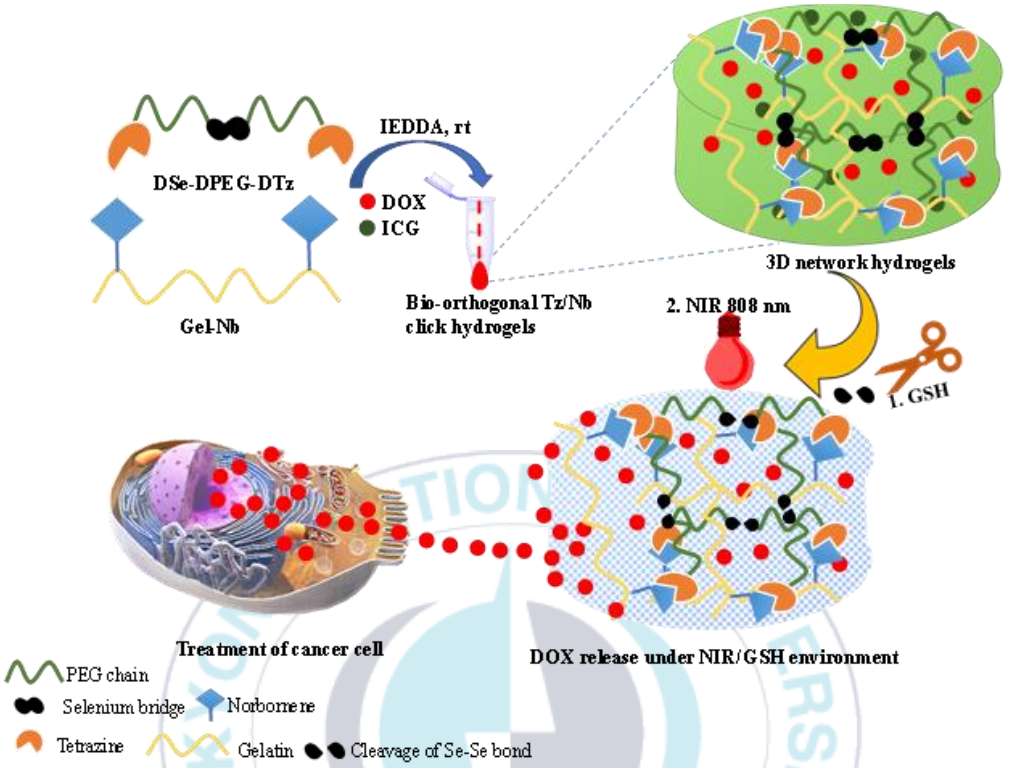

Scheme 1 Theschematic of the synthesis of dual-responsive gelatin-based hydrogels and mechanistic pathway for cleavage of diselenide bonds under the influence of reduction/NIR stimuli and drug release.

2.2. Experimental

2.2.1. Materials

Gelatin porcine skin (Type A 300 Bloom, MW. 100 kDa), N-hydroxy succinic acid (NHS, 98%), and glutathione (GSH) were procured from Sigma Aldrich (Korea). 5-Norbornene-2-carboxylic acid (Nb-COOH, ≥98%,), N-(3-dimethyl aminopropyl)-N′-ethyl carbodiimide hydrochloride (EDC. HCl, 99%), ICG were bought from Tokyo Chemical Industry (Japan). DOX. HCL was bought from TargetMol Chemicals Inc. (USA). 2,2'-((Diselanediylbis (ethane-2, 1-diyl)) bis(poly(oxyethylene) (DSe-DPEG), 5-((4-(1,2,4,5-tetrazine-3 yl)benzyl)amino)-5-oxopentanoic acid (Tz-COOH), and di-selenide-di-polyethylene glycol-di-tetrazine (DSe-DPEG-DTz) were prepared by referring to our previous reports (Fig. 2) [45] and their ^{1}H-NMR/FTIR spectra were presented in Fig. 3 (a-c) and Fig. 4 (a-c) respectively.

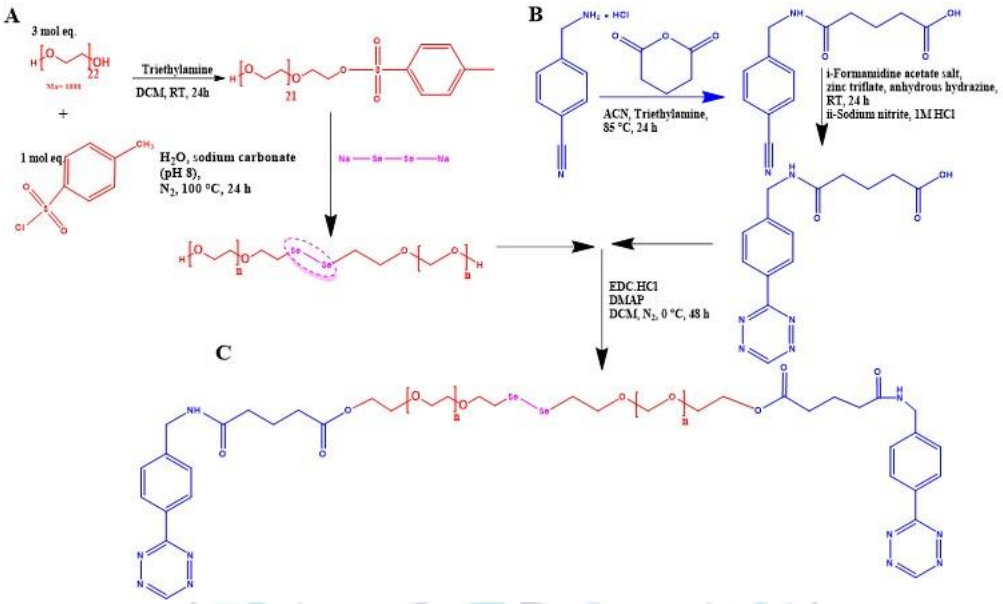

Fig. 2 Synthetic route for DSe-DPEG-DTz

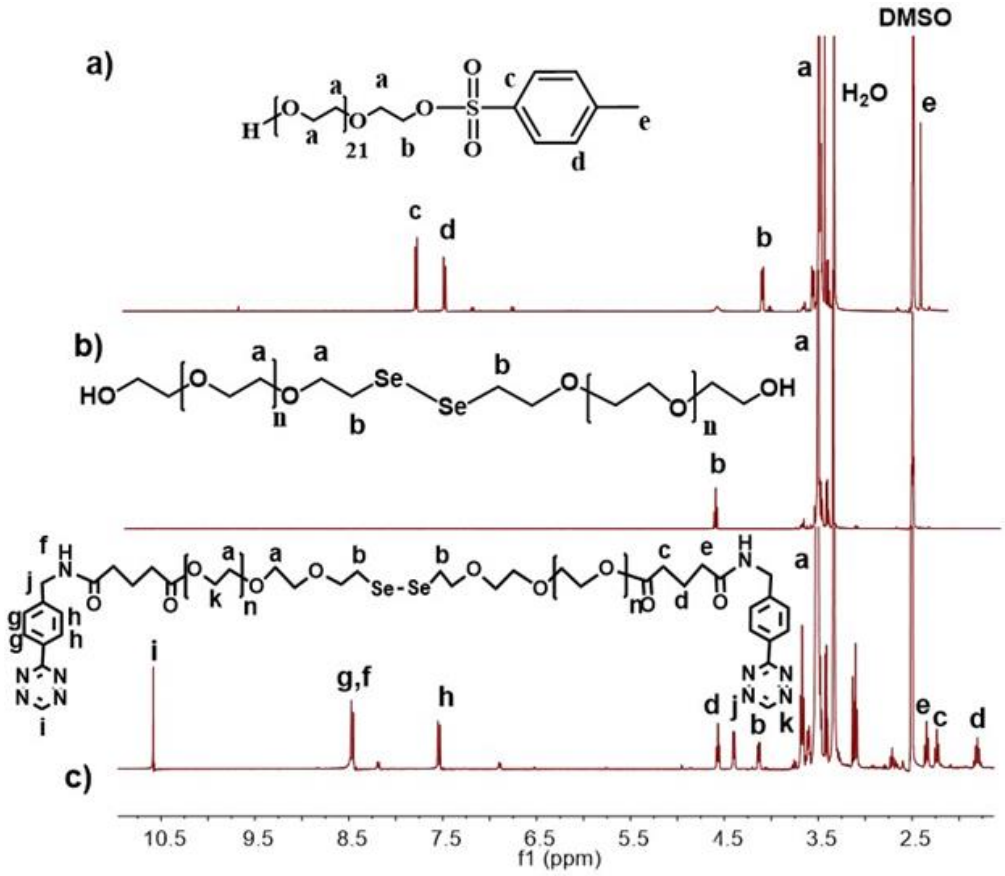

Fig. 3 ^{1}H-NMR spectra of (a) PEG-tosyl, (b) DSe-DPEG, and (c) DSe-DPEG-DTz.

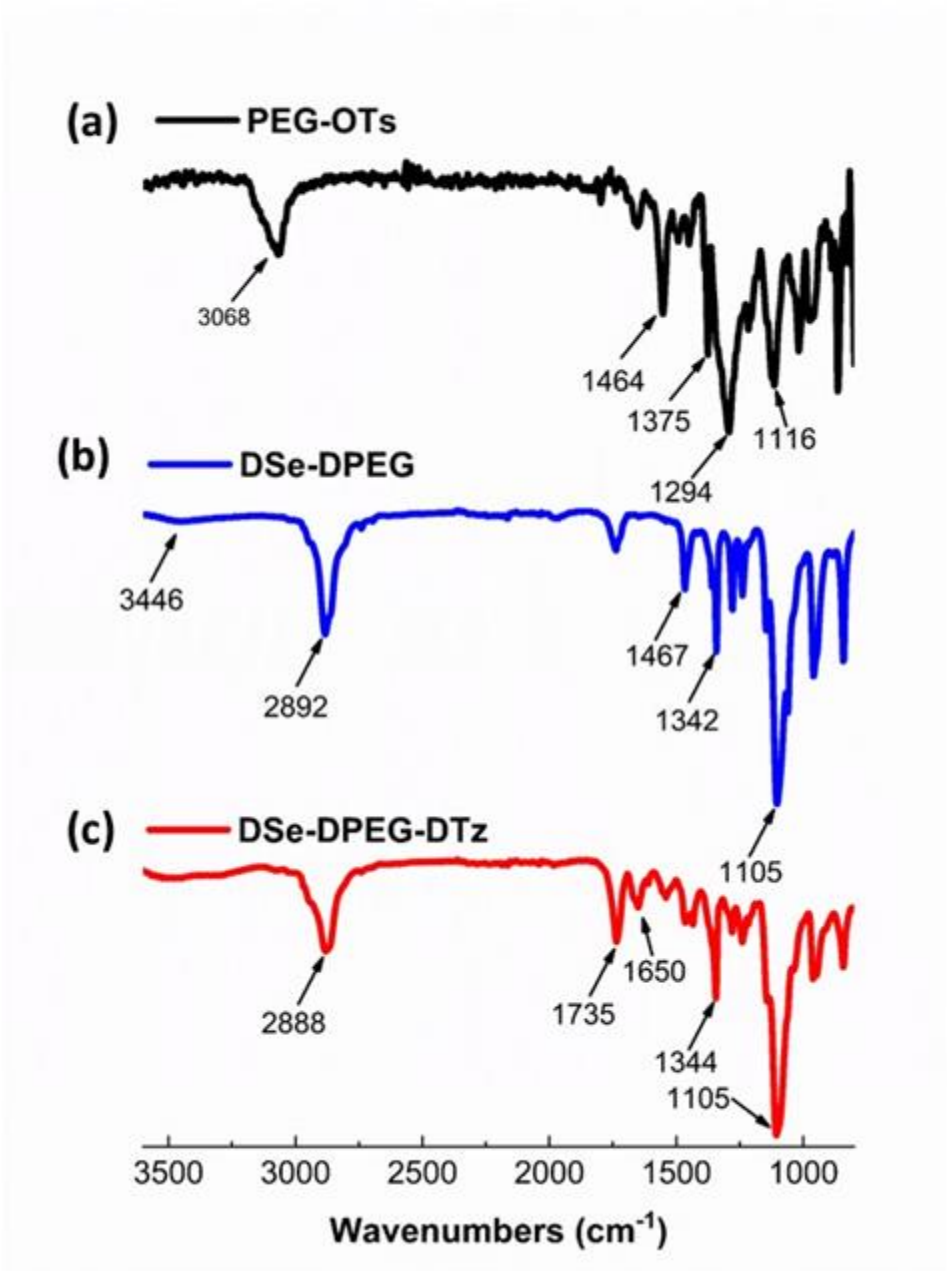

Fig. 4 FTIR spectra of (a) PEG-OTs, (b) DSe-DPEG, and (c) DSe-DPEG-DTz

2.2.2. Instruments

Nuclear magnetic resonance (NMR) analyses were carried out using a JEOL NMR spectrometer (JNM ECZ-400). The UV-vis spectrophotometer (Optizen POP) was used for drug release measurements. A low vacuum scanning electron microscope (LV-SEM, JEOL, Gatan, JSM-6490LV) was used to inspect the cross-sectional images of hydrogels. Viscoelastic property of hydrogels was studied by means of a Discovery HR-2 hybrid rheometer (TA instrument).

2.3. Preparation of precursors for hydrogel formulation

2.3.1. Preparation of precursors for hydrogel formulation

Gel-Nb was prepared by using a published protocol with a little variation, as shown in Scheme 2 [46]. Briefly, 3.84 mmol of Nb-COOH (dissolved in DCM) was added to EDC.HCl (3.84 mmol). After 10 min, NHS (5.76 mmol) was put into the reaction mixture and stirred for 24 h at RT to make NHS active ester. The solution was filtered and concentrated by a rotary evaporator and then dissolved in 10 mL of DMSO. In parallel, 0.5 g of gelatin A (3.84 mmol of NH_2) was dissolved in a preheated (40 °C) sodium bicarbonate buffer (pH 8) solution and stirred for 1 h, then it was allowed to mix homogenously overnight at RT. Both mixtures (the NHS active ester and gelatin solution) were allowed to react for next 24 h. Consequently, the crude product was obtained by precipitation in acetone (7-10 folds). The precipitates were re-dissolved in water to get a homogenous solution and eventually the solution was dialyzed (MWCO12-14 KDa) for 3 d at RT by changing the DI water each 8 h. The white spongy product was obtained by lyophilization. The modification of gelatin with Nb was elucidated by ^{1}H-NMR spectroscopy.

2.3.2. Determination of the free-amine content of gelatin and the degree of substitution of Gel-Nb

The free amine content of gelatin and the degree of substitution (DS) of Gel-Nb was evaluated by a ninhydrin assay according to a modified protocol described previously [47]. Concisely, 4 mg of gelatin and lyophilized Gel-Nb samples were mixed in DI water (2 mL) and 1 mL of freshly prepared 2% ninhydrin solution (in ethanol). The solution mixture was allowed to heat at 100 °C (30 min) and cooled with cold water to end the reaction. The resulting blue-purple complex showed an absorption maximum at 570 nm. The free amine content of gelatin was determined with the help of glycine as a standard amine compound. A standard curve was made after reacting different concentrations of glycine with the ninhydrin solution (Fig. 5). The calculation for DS was carried out by using the following equation:

$$DS\ (\%) = (1 - \frac{Am}{Au}) \times 100 \quad (1)$$

A_m and A_u represent the absorption of modified gelatin with Nb and un-modified gelatin, respectively. DS was determined to be 55% of original amine contents.

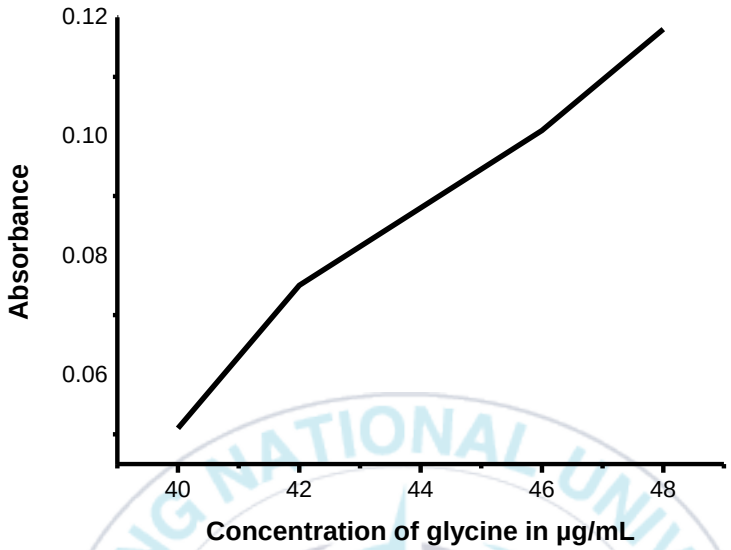

Fig. 5 Glycine standard curve for determination of free-amine contents in gelatin by Ninhydrin assay.

2.4. Formulation of hydrogel

Gelatin-based hydrogels were formulated through the reaction of the cross-linker (DSe-DPEG-DTz) and Gel-Nb. Briefly, homogenous solutions of Gel-Nb (10%) in DI H_2O and DSe-DPEG-DTz (dissolved in DI H_2O) were mixed in vials according to different molar ratios (10:10, 10:5, 10:2.5 with respect to Nb:Tz) as presented in Table 1. The images of formulated hydrogels in the vials and confirmation of injectability were presented in Fig. 6b and c, respectively. The gelation time of the cross-linked hydrogels was determined by using a digital stopwatch while inverting the vials. The porous morphologies of the hydrogels were confirmed by a LV-SEM.

Table 1 Composition and gelation time of hydrogels.

Sr. No.	Hydrogel Code	Nb:Tz[a] (mmol)	Gelation Time (sec)[b]
1	GHG-A	10:2.5	523 ± 90
2	GHG-B	10:5	380 ± 55
3	GHG-C	10:10	170 ± 30

[a] Theoretical mol equivalent of Nb and Tz moieties

[b] Gelation time estimated by the vial inversion method at room temperature

2.5. Characterization

2.5.1. Rheological properties of gelatin hydrogels

The rheological measurement of gelatin-based hydrogels was carried out by dynamic oscillation of two parallel plates to determine storage moduli (G′) and loss moduli (G″). 200 µl of a Gel-Nb solution (10% w/v) in DI H_2O containing DSe-DPEG-DTz was injected between the plates with a gap setting of 250 µm to check the frequency sweep of the hydrogels. The frequency sweep was carried out at varying angular frequencies (0.1 to 100 rad/s). The gelation time of the hydrogels was monitored for 600 s to evaluate G′ of cross-linked hydrogels.

2.5.2. The swelling study of gelatin hydrogels

The swelling property of hydrogels was assessed by a gravimetric method. Lyophilized hydrogels were immersed in an adequate amount of PBS solution (pH 7.4) at physiological temperature. The weight of swollen hydrogels was taken at intervals of time until equilibrium in weight was achieved. The experiment was carried out in triplicate for each hydrogel. The following equation was used to calculate the equilibrium swelling ratio (ESR).

$$\text{ESR } \% = (\text{Ms} - \text{Md}/\text{Md}) \times 100 \quad (2)$$

Where, Ms is the mass of swollen hydrogels and Md is the mass of the lyophilized hydrogels.

2.5.3. Morphology of gelatin hydrogels

The SEM investigation was accomplished to assess internal morphologies of the prepared hydrogels. Hydrogel samples were lyophilized and cut vertically in liquid N_2 before the analysis.

2.5.4. The drug loading and release experiments

For the preparation of drug-encapsulated hydrogels, DOX (1mg/mL) and DOX (1mg/mL) + ICG (1 mg/mL) were first dissolved with Gel-Nb (10% in DI H_2O) in microcentrifuge tubes. DSe-DPEG-DTz (in DI H_2O, Nb:Tz = 10:10) was transferred to each tube and the components were shaken mildly using a vortex mixer for 20 s at RT to form AR1 (description is given in Table 2) and AR2. The drug-loaded lyophilized hydrogels were rinsed with PBS solutions to draw out the unloaded drug from the surface prior to evaluate the loading efficiency and drug release profiles.

For a drug release study, the drug-encapsulated hydrogels were placed in PBS (pH 7.4) solution containing 10 mmol of GSH. Furthermore, NIR-responsive drug release studies were performed by irradiating NIR light to the hydrogels in PBS (pH 7.4) for 10 min at 2 W power. The drug release was performed in a dialysis bag (3500 MWCO) having 5 mL of the dissolution medium followed by dialyzing against 30 mL of the release medium (37°C and 100 rpm). At definite time intervals, aliquots of 3 mL were taken from the dissolution medium followed by the addition of 3 mL of the fresh medium. The % of DOX release was measured through a UV-vis spectrophotometer at the wavelength of 485 nm by using the standard curve of DOX in PBS with or without GSH (10 mmol). The drug loading efficiency (DLE) was determined by the following equation.

$$\text{Drug loading efficiency (\%)} = \frac{(\text{wt of drug in feed} - \text{wt of drug in supernatant})}{\text{weight of total drug}} \times 100 \quad (3)$$

The percent of drug released (%) was calculated with the following equation.

$$\textit{The percent drug release}\ (\%) = \frac{\textit{Total released DOX}}{\textit{Total DOX in hydrogels}} \times 100 \quad (4)$$

Table 2 Drug release/anticancer/live-dead assay conditions with their corresponding codes

Sr. No.	Code	Drug release/anticancer/live-dead assay conditions
1	AR1	DOX@GHG-C (PBS pH 7.4)
2	AR2	DOX+ICG@GHG-C (PBS pH 7.4)
3	AR3	DOX@GHG-C (GSH 10 mM)
4	AR4	DOX+ICG@GHG-C (GSH 10 mM)
5	AR5	DOX+ICG@GHG-C (NIR: OFF)
6	AR6	DOX+ICG@GHG-C (NIR: ON)
7	AR7	DOX+ICG@GHG-C (GSH 10 mM & NIR: ON)

2.5.5. *In vitro* cytocompatibility analysis of the precursors and prepared hydrogels

The human embryonic kidney cell line (HEK-293) was used to examine the cytocompatibility of Gel-Nb, DSe-DPEG-DTz, and the resulting hydrogels with the help of water-soluble tetrazolium salt (WST) assay (EZ-cytox, South Korea). The cells were grown in DMEM supplied with 10 % fetal bovine serum (FBS) and 1% antibiotic-antimycotic solution in an incubator at 37°C with 5% CO_2 for 48 h, and passaged to a 48 well plate at a seeding density of 10^4 cells per well. Afterward, the culture media were drawn and substituted with fresh culture media containing Gel-Nb (250-4000 µg/mL) and DSe-DPEG-DTz (25-200 µg/mL). After 48 h, the cells were washed twicewith PBS (100 µL). Finally, a fresh medium including the solution of WST assay (10 µL) was added into each well. The viability of the cells was measured through the determination of optical density at a wavelength of 450 nm through a microplate reader.

2.5.6. Anti-cancer activity of the DOX-encapsulated hydrogels

The anti-cancer ability of the DOX-encapsulated hydrogels was evaluated through WST assay using BT-20 cell line. The cells were cultured and seeded in a 48-well plate. The culture medium was then drawn off and substituted with a fresh medium having 10 mmol of GSH. Afterwards, the cells were given treatment with free DOX and AR1 (by floating hydrogels on the cell culture medium) for 48 h. For NIR-responsivity, AR2 on the cell culture medium without GSH were irradiated with NIR light (808 nm, 3 min, 2 W power).

2.5.7. Fluorescence based live/dead assay

The cellular live and dead assays of blank hydrogels, AR1 (40 µg equiv. of DOX), AR2 and free DOX solution (40 µg) were examined on BT-20 cells. The

cells after the above-mentioned treatments were dyed with calcein-AM to identify viable cells (green) followed by staining of ethidium bromide for detecting the non-viable (red) cells through fluorescence microscopic technique.

2.5.8. Degradation studies of the hydrogels

The hydrogel degradation pertaining to the weight loss of the gels was estimated through the gravimetric method for a total period of 8 d. The pre-weighed hydrogels were placed in the relevant stimulus applied dissolution medias including PBS pH 7.4, GSH (10 mM), and NIR irradiation. The gels were removed after a specific interval of time, blotted the surface water molecules and lyophilized. The dried gels were weighed again with analytical balance. The percent weight loss was calculated through the following equation.

$$Weight\ loss\ (\%) = \frac{Wd-Wr}{Wd} \times 100 \quad (5)$$

Where, Wd indicates the weight of dry hydrogel while Wr shows the remaining weight of the hydrogel.

2.5.9. Statistical analysis

All physiochemical studies were carried out in triplicate while cell culture assays were accomplished by using 4 replicas, and data are expressed as mean ± standard deviation.

2.6. Results and Discussion

2.6.1. Synthesis of Gel-Nb

The primary amines at gelatin backbone can act as a nucleophile, and therefore, can react with the COOH functional group of Nb-COOH. Prior to the modification reaction, the primary amine content (8%) of gelatin was calculated using a ninhydrin assay (Fig. 5). In order to prepare Gel-Nb, we opted a two-step bioconjugation process (Scheme 2B). Firstly, *in situ* NHS active esters was prepared from Nb-COOH, and the residues of EDC and NHS were removed by using filter paper. The esters was further reacted with a gelatin solution (pH≈8-9) to obtain Gel-Nb [46]. The conjugation of gelatin with Nb occurred by an amide linkage formation between the amine and carboxylic acid groups. The quantity of the unreacted NH_2 groups in gelatin was measured by a ninhydrin assay and was used to calculate DS, which was found to be 55% (Fig. 4). ^{1}H-NMR confirmed the presence of Nb functional groups at 6.03-6.10 ppm in the spectrum of Gel-Nb (Fig. 6a). For sake of conserving gelatin bioactivity after chemical modification with Nb, a low DS is suitable because the remaining primary amine groups could be useful for cellular recognition [48]. Conclusively, Gel-Nb was effectively synthesized having the ability to form hydrogels.

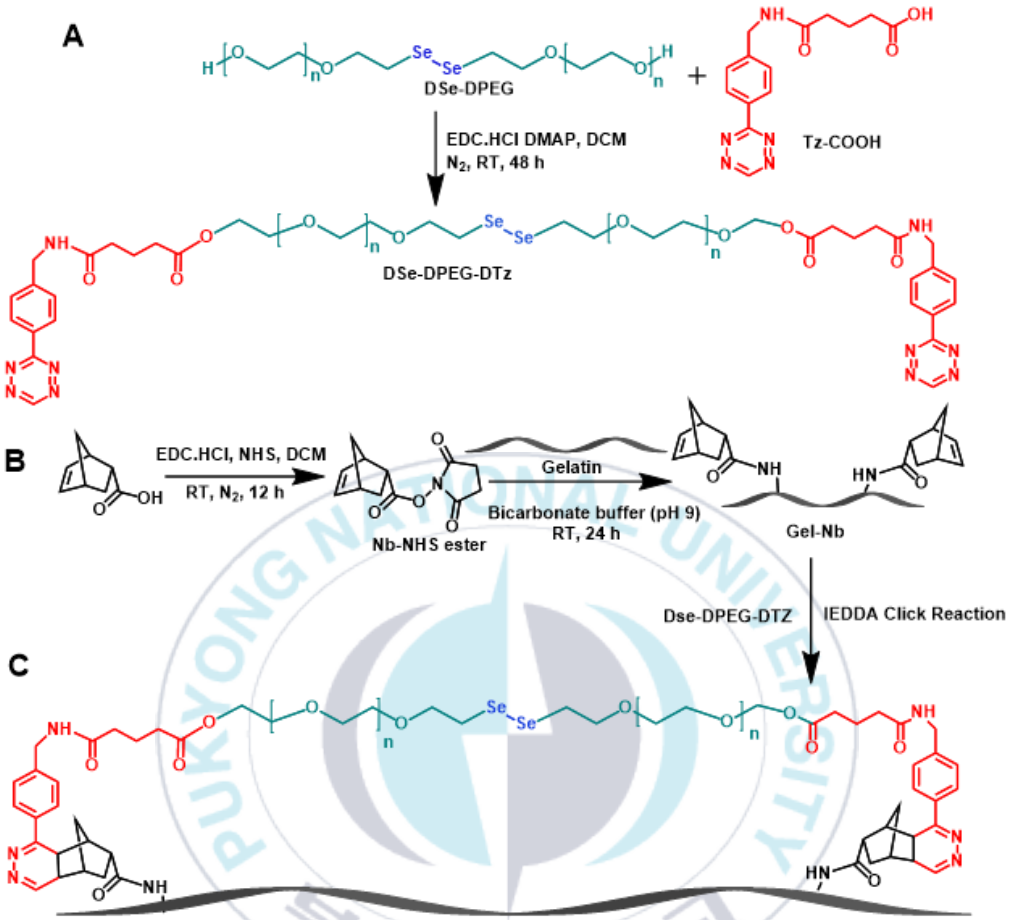

Scheme 2 The synthesis pathway of the active precursors. (A) Chemical synthesis of the dual-responsive cross-linker (DSe-DPEG-DTz), (B) chemical modification of Gel-Nb using EDC chemistry, and (C) cross-linking of Gel-Nb with dual-responsive cross-linker (DSe-DPEG-DTz).

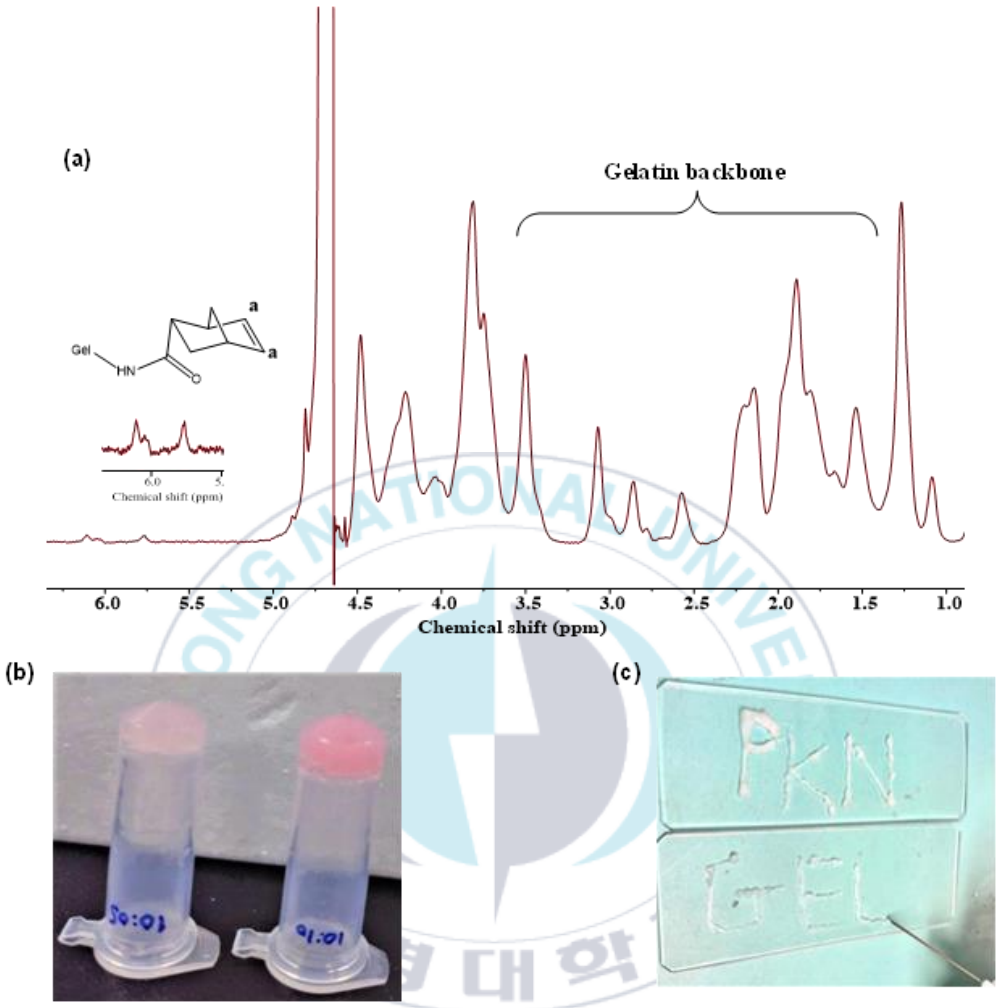

Fig. 6 Characterization of modified gelatin and injectability of hydrogels. (a) ^{1}H-NMR of Gel-Nb. (b) Images showing the formulation of hydrogels with varying concentration of cross-linker. (c) Image showing injectability of hydrogels.

2.6.2. Preparation and rheological properties of gelatin hydrogels

To formulate hydrogels, a homogenous solution of Gel-Nb (10% w/v in DI) was mixed with different feed ratios (10:2.5, 10:5, and 10:10 of Nb:Tz mol. ratio) of the cross-linker, DSe-DPEG-DTz. The quick IEDDA click reaction of the Tz and Nb moieties took place after stirring the solutions through a vortex mixer, resulting in the gelatin hydrogels in a short time (few minutes), which was considered an appropriate time for injecting the hydrogel through a needle. The FT-IR spectrum of the hydrogels (Fig. 7) represented the characteristic peak of alkene bonds (C=C) of Tz at 1640 cm^{-1}, confirming the incorporation of Tz moieties *via* the IEDDA reaction. The hydrogels were designated as GHG-A, GHG-B, and GHG-C according to their increasing molar concentration of the cross-linker. Thus, the hydrogels comprised different cross-linking densities. The gelation speed was affected by the concentration of the cross-linker and Gel-Nb solution. It was noted that a higher ratio of DSe-DPEG-DTzto Gel-Nbled to a faster time of gelation, which could be credited to the fast click reaction of IEDDA, rendering the efficient conversion in the absence of any catalyst [29]. Precisely, the gelation time of GHG-A (10:2.5 of Nb:Tz) was measured 523 s, which was decreased to 170 s with the enhancement of the cross-linker molar feed ratio to 10:10 (GHG-C) as shown in Table 1. It could be recognized that the altering of the ratio of Gel-Nb and DSe-DPEG-DTz led to varied gelation times of the prepared hydrogels.

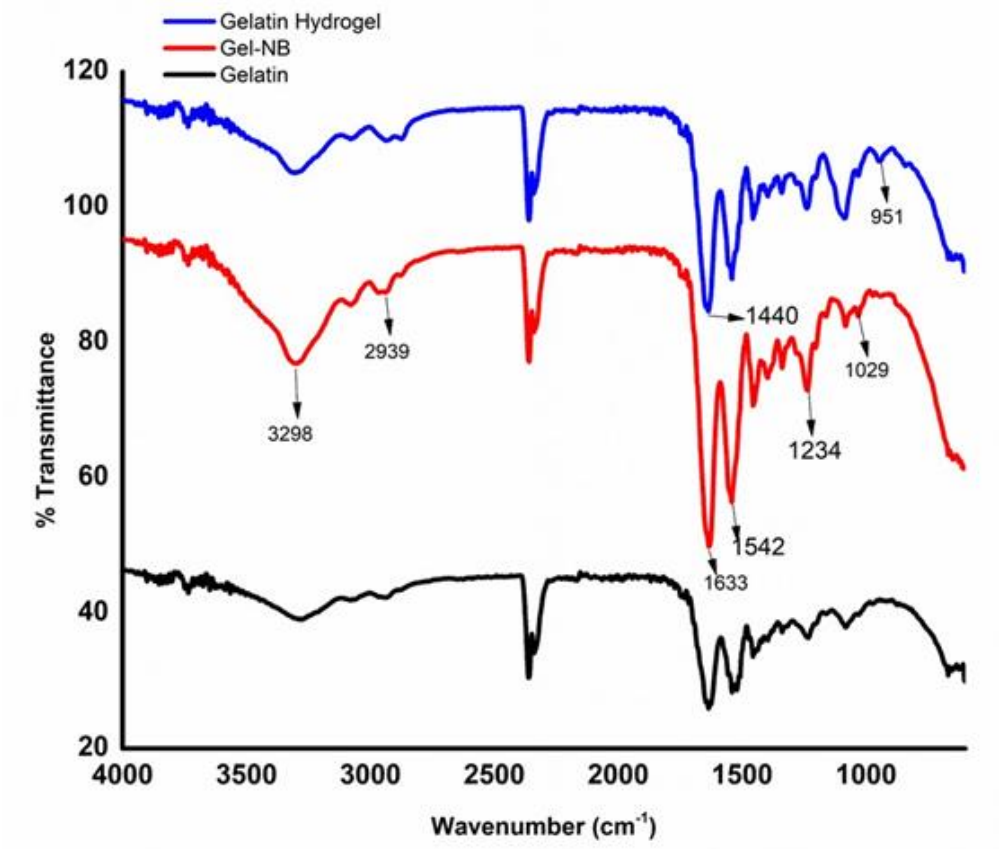

Fig. 7 FTIR spectra of gelatin, Gel-Nb, and gelatin hydrogels

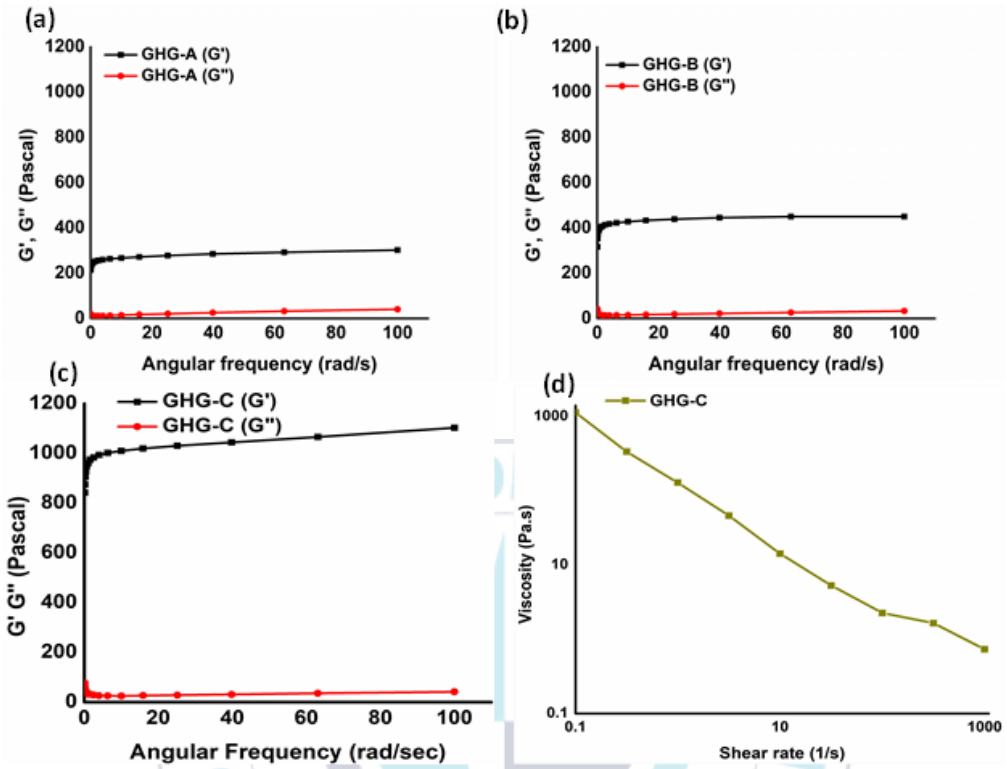

Fig. 8 Rheological features of hydrogels (a-c), storage and loss modulus of GHG-A, GHG-B, and GHG-C as a function of respective angular frequency. (d) Shear viscosity of GHG-C as a function of shear rate at 25 °C.

The rheological aspects of injectable hydrogels play a vital role in local drug delivery systems [32]. We assessed the mechanical stability of the gelatin-based hydrogels through measuring the storage modulus (G′) and loss modulus (G″) along with shear thinning properties. The obtained values were then plotted against angular frequency (Fig. 8a-c). The shear viscosity values of GHG-C were plotted against shear rate as shown in Fig. 8d while the other two formulations were shown in Fig. 9a-b.

In the frequency sweep analyses, G′ was always higher than G″, representing elastic nature of the prepared hydrogels. The G values of GHG-A, GHG-B, and GHG-C were shown to be 300, 450, and 1100 Pa, respectively. Hence, the mechanical strength of the hydrogels was highly dependent upon the molar feed ratio of the cross-linker to Gel-Nb. This result denotes that a tuning of the cross-linker concentration allows the fabrication of hydrogels that mimic the tissue mechanics broadly (0.1-100 kPa) [49]. GHG-C (Tz/Nb of 10:10) showed the maximum G′ of 1100 Pa, indicating the highest mechanical strength, thus this composition was used in the experiment of drug release and anti-tumor activities.

For shear thinning property, the shear viscosity of hydrogels was plotted as a function of shear rate. All the hydrogels exhibited a gel-to-sol transition (non-Newtonian flow), as shown in Fig. 8d and Fig. 9 (a-b). When shear tress was applied onto the hydrogels, the viscosity of the samples reduced in direct proportion. At reaching a certain shear rate (>4.0 s^{-1}), the viscoelastic sample was incapable to return to its original state and its viscosity became lower.

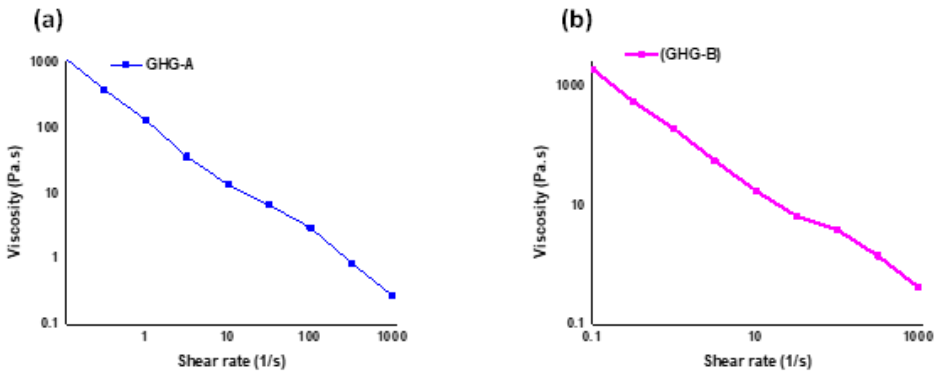

Fig. 9 Shear viscosity of the GHG-A and GHG-B hydrogels versus shear rate at 25 °C.

2.6.3. The swelling studies of the hydrogels

Swelling property is an important feature of hydrogels used in biomedical applications. The time to reach equilibrium and dynamic swelling are paramount aspects because they can affect drug loading capacity and drug release kinetics. The swelling ratios (%) of the hydrogels GHG-A, GHG-B, and GHG-C are depicted in Fig. 10. After cross-linking, the % swelling ratio was measured by immersing the pre-weighed lyophilized hydrogels in the PBS solution (pH 7.4) for 72 h until equilibrium in weight was achieved. It was found that the concentration of the cross-linker had an inverse effect on the swelling behavior. By reducing the quantity of DSe-DPEG-DTz, the swelling of the hydrogels was raised gradually. A higher concentration of cross-linkers led to denser networks which allowed less penetration of water [35]. All the hydrogels (GHG-A, GHG-B, and GHG-C) showed dynamic swelling during the initial 12 h, with the swelling ratios of 1456, 1301, and 1253%, respectively. The quick water uptake of the hydrogels in the early stages is likely due to the presence of micropores and polyethylene glycol (PEG) hydrophilic chains present in the cross-linker. These findings are in accordance with the earlier works [50-51]. Furthermore, the hydrogel GHG-A has a lower cross-linking density presenting a loose network and water can easily be diffused as compared to the hydrogels GHG-B and GHG-C with higher cross-linking densities.

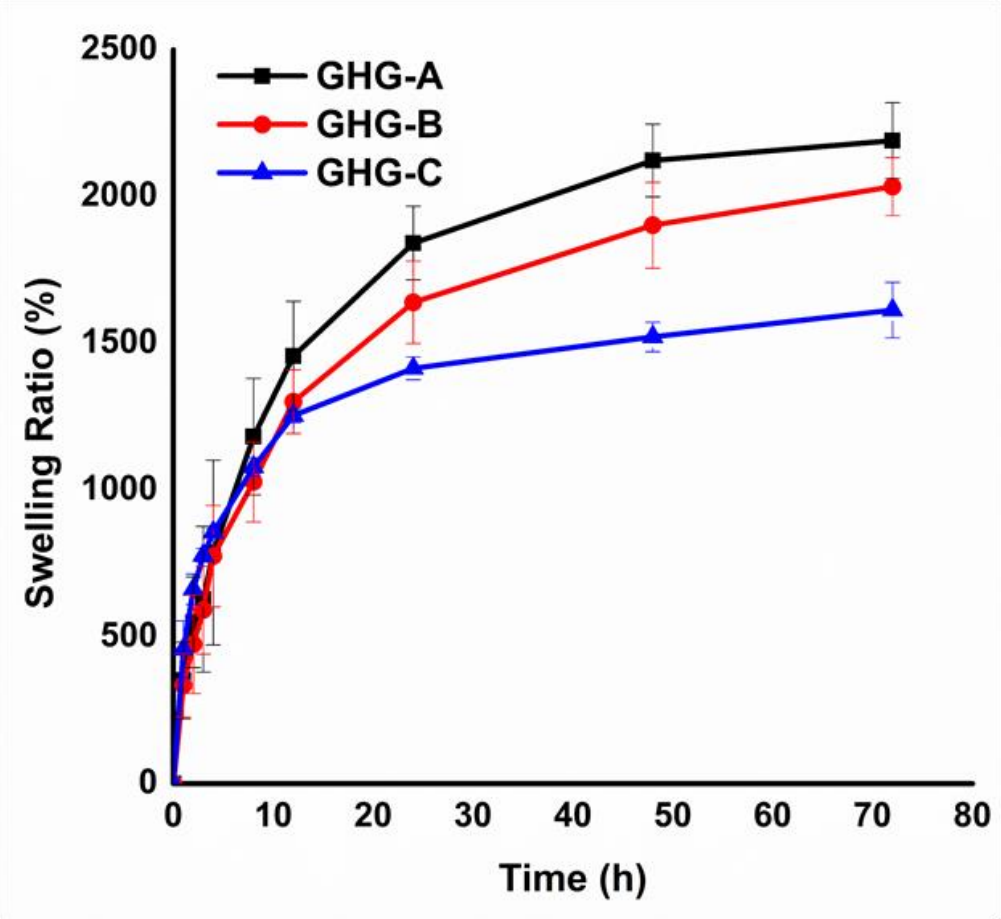

Fig. 10 The Swelling capability of hydrogels in PBS (pH 7.4).

2.6.4. Morphological analysis

Injectable hydrogels with porous architectures may serve as a potential candidate for drug delivery, bioprinting and tissue engineering applications. The cross-sectional SEM images of the gelatin-based hydrogels with different cross-linking densities are shown in Fig. 11(a-c). Each formulated hydrogel exhibited porous morphologies in the micrometer range. These porous architectures could be attributed to the production of the *in-situ* N_2 gas within the hydrogel networkas well as thelyophilization process. The IEDDA reaction between Tz and Nb (strained alkene) moieties occurs rapidly under physiological conditions yielding covalent links. This click chemistry reaction produces only N_2 gas as a byproduct which is useful for the pore generation inside the hydrogel network. The size of porous structure of the hydrogels was found to depend upon the cross-linking density, as depicted in Fig. 11(a-c). The hydrogel GHG-C presented average pore sizes of approximately 77 μm with highest cross-linking density (Fig. 11c). Meanwhile, GHG-B and A showed bigger average pore sizes of 86 and 97 μm respectively due to lower cross-linking densities (Fig. 11b & a). Consequently, these hydrogels can easily swell facilitating the release of the drug molecules [44].

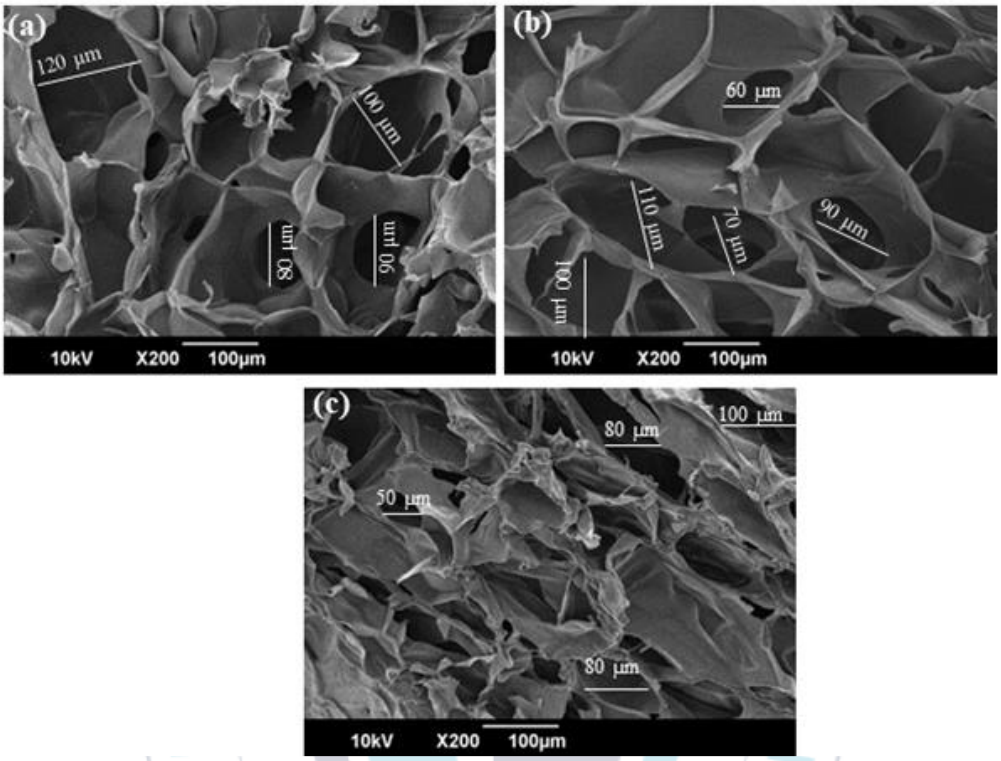

Fig. 11 The scaning electron photomicrographs of the hydrogels, (a) GHG-A, (b) GHG-B, and (c) GHG-C at magnification of 200X (10kV).

2.6.5. *In vitro* drug loading and release studies

The drug loading efficiency was calculated by measuring absorbance of DOX in UV-visible spectrophotometry. All the hydrogels displayed maximum drug loading efficiency above 90% possibly due to the highly porous structure. The interactions between the carboxylate groups (negative charge) of gelatin and ammonium ions (positive charge) of DOX could also facilitate the enhanced loading efficiency [45].

The drug release was performed in PBS (pH 7.4) and reducing media (with 10 mmol of GSH) at 37°C mimicking the tumor environment (Fig. 12a). The drug release experiment was also accomplished after exposing the hydrogel to NIR light, as shown in (Fig. 12b). For this experiment, ICG was co-encapsulated as a ROS generator along with DOX. The hydrogel GHG-C of maximum cross-linking density was opted for the *in-vitro* drug release test. In PBS (pH 7.4), AR1, AR2 and AR5 showed nominal and restrained DOX release (Fig. 12a, b). The images of drug release under the dual responsive environments are displayed in Fig. 13-14.

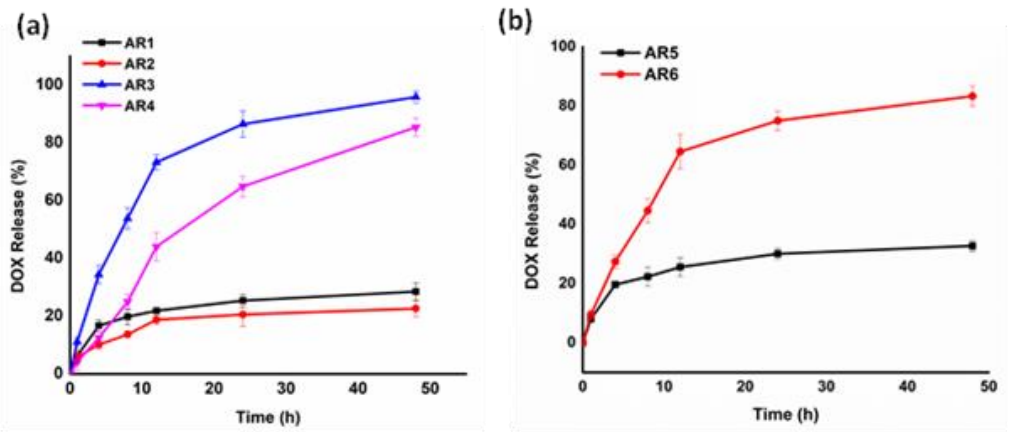

Fig. 12 The in vitro DOX release profile of (a) AR1 and AR2 in PBS pH 7.4, AR3 and AR4 in GSH 10 mM (b) DOX release from AR5 and AR6 in respected NIR: OFF, and ON conditions.

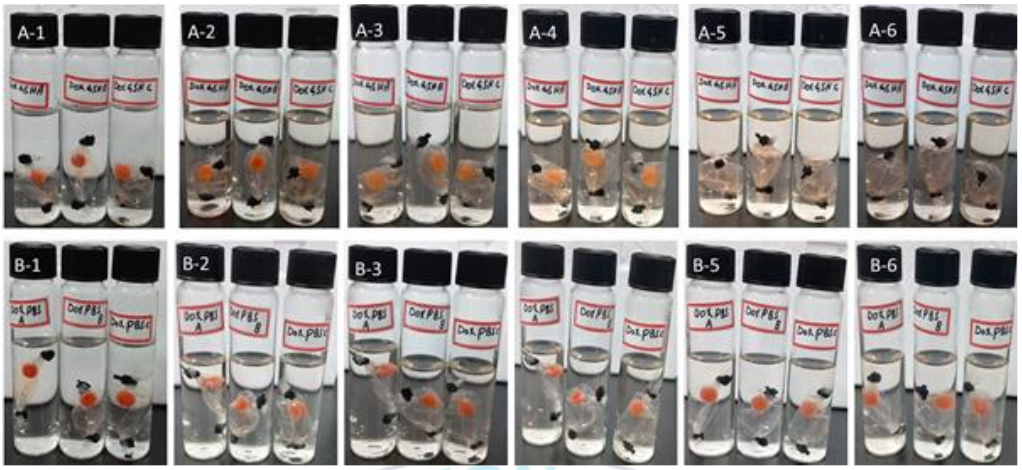

Fig. 13 DOX release from AR3 under GSH (10mM) in 1h, 4h, 8h, 12h, 24h, and 48h (A-1 – A-6) and DOX release from AR1 in PBS (pH7.4) in 1h, 4h, 8h, 12h, 24h, and 48h (B-1 – B-6).

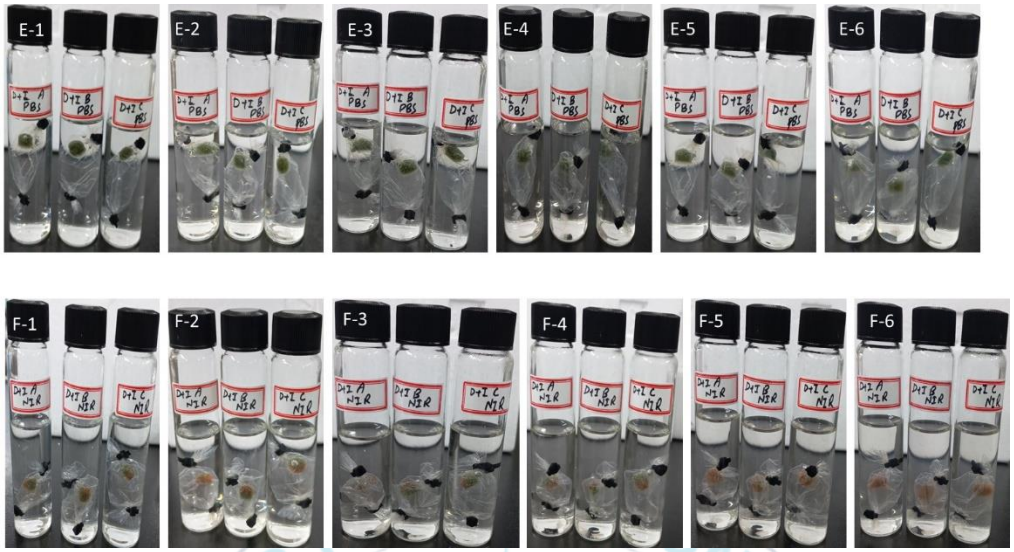

Fig. 14 DOX release from AR5 in PBS (pH 7.4) in 1h, 4h, 8h, 12h, 24h, and 48h (E-1 – E-6) and DOX release from AR6 after exposure to NIR radiation in 1h, 4h, 8h, 12h, 24h, and 48h (F-1 – F-6).

It is observed that <30% of drug contents were released from AR1 and AR2 under physiological conditions (Fig. 12a). When AR3 was incubated in the reducing environment (with 10 mM of GSH), more than 95% DOX was released while ca. 80% of DOX was released from AR4, indicating the evidence of the reduction-responsive behavior of the gelatin hydrogels. It is also notable that the burst release (ca. 73%) occurred in 12 h from AR3, followed by the sustained release for next 28 h in reducing environment. This sharp drug release can be primarily attributed to the cleavage of the Se-Se bond of the cross-linking in the hydrogel network, which consequently encouraged the DOX release by disintegration of the interior network [34]. The relatively low drug release from AR4 compared to AR3 might be due to the interaction of ICG and DOX molecules, which hindered the DOX release from the hydrogels [52]. The hydrogel feed composition and applied external stimuli play a significant role in deciding the cumulative release of the enclosed drug molecules. Contrary to the findings of a study [53], our hydrogel formulation (AR1) liberated 30% of the DOX molecules at physiological pH justifying the tunability of the hydrogels based on feed composition and physicochemical properties for targeting the various pathological conditions.

To confirm the NIR-responsive behavior of the gelatin hydrogels, we performed the drug release experiment under NIR (2 W/cm^2) irradiation. Here, AR5 and AR6 were assessed for the experiment. The fast release (ca. 60%) of DOX from AR6 was detected in 12 h after exposing the hydrogels to NIR irradiation and a temporal and steady release of DOX was observed for next 36 h to reach the maximum of 82%, as shown in Fig. 12b. In contrast, 26% of DOX release was detected from AR5 after 48 h without NIR irradiation. It is considered that the NIR light-induced ROS from ICG, which cleaved the diselenide bonds in the

hydrogel network, resulting in the quick release of the encapsulated DOX [35]. The combined effect of NIR and GSH on the hydrogels release profile is shown in (Fig. 15), revealing that the amount of DOX released under combined effect in 24 h is similar to that from AR3 formulation in GSH medium (Fig. 12a). It is assumed that the reduction stimulus of 10 mM of GSH dominates the de-crosslinking reaction and the combined effect of GSH and NIR was not significant in terms of DOX release from the hydrogel system.

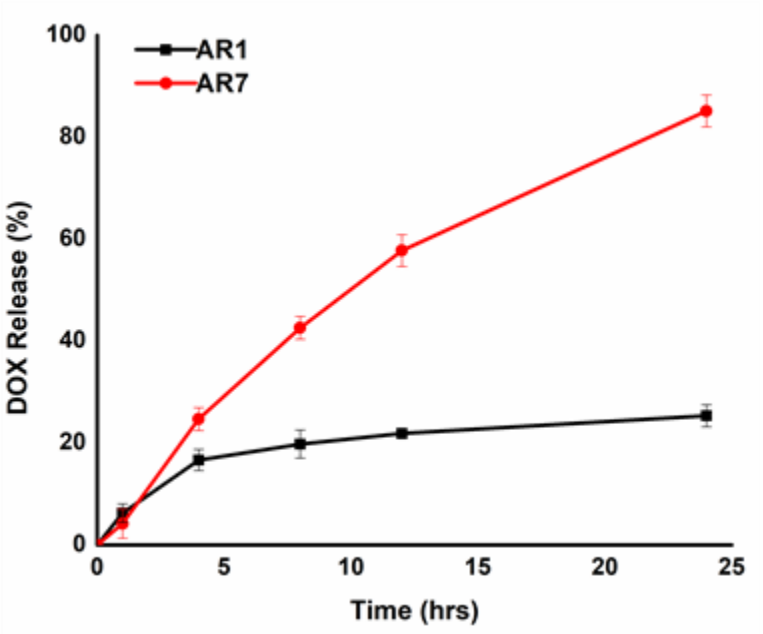

Fig. 15 The combined effect of NIR and GSH on the in vitro DOX release profile of AR7.

The important parameters which need to be considered while formulating a delivery system include solubility of the drug molecules, drug diffusion and erosion capability of the polymer components. The release of the drug molecules from biological source polymers like gelatin is supported by diffusion and erosion processes of the polymer networks [54]. Different mathematical

models were applied on the DOX release data including zero order, first order, Higuchi model and Peppas model (Fig. 16) to find out the best regression fit (R^2) which is closer to 1. The value of Higuchi model R^2 was closer to 1 (Table 3), indicating that DOX release follows the Higuchi pattern of released facilitated by Fickian diffusion process. The value of n representing the slope of Peppas model is >1, hence the DOX release was following the super case transport-II mechanism involving the erosion and diffusion processes except AR7 (combined stimulus) which follows the anomalous diffusion mechanism [55].

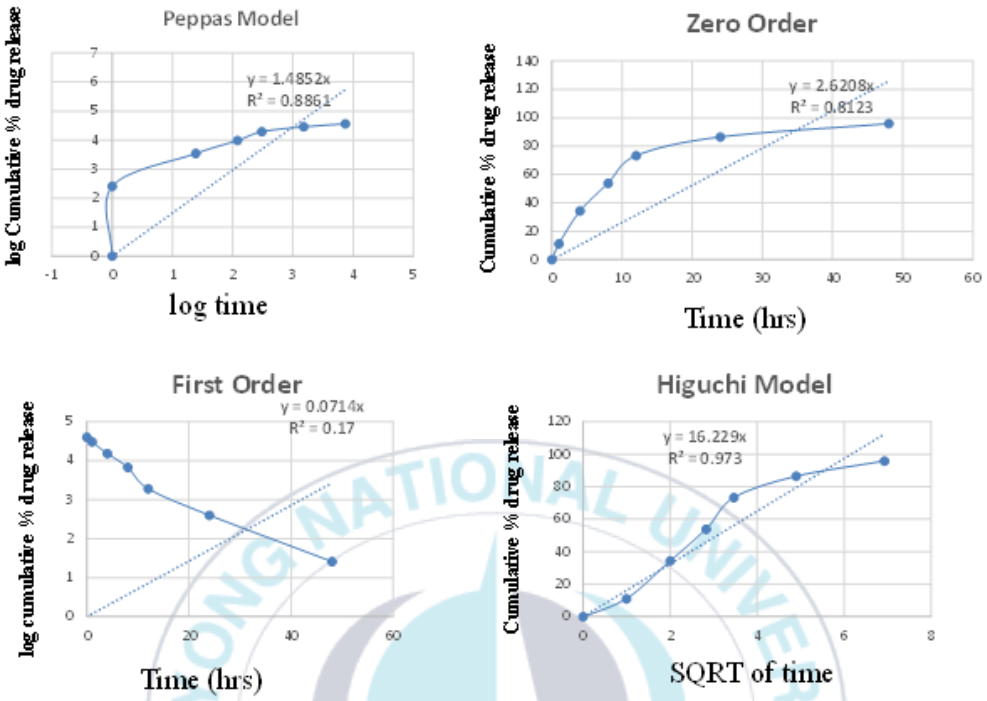

Fig. 16 Sample AR3 drug release data fitted to various kinetic models. Peppas, zero order, first order, and Higuchi model

Table 3 Mechanism of DOX release in dissolution experiment with different release conditions.

Sr. No	Code	Zero Order (R^2)	First Order (R^2)	Higuchi (R^2)	Peppas model (R^2)	*n* value
1	AR1	0.7435	0.4126	0.9482	0.873	1.0936
2	AR2	0.768	0.4169	0.9598	0.8804	1.003
3	AR3	0.8123	0.170	0.973	0.8861	1.4852
4	AR4	0.9377	0.2182	0.9774	0.9512	1.3354
5	AR5	0.8181	0.2870	0.9728	0.8932	1.4316
6	AR6	0.7387	0.4086	0.9464	0.8616	1.1457
7	AR7	0.9693	0.3409	0.9808	0.7946	0.2492

* *n*, slope of Peppas model

2.6.6. *In vitro* cytocompatibility of Gel-Nb, cross-linker, and hydrogels

The cytotoxic properties of Gel-Nb, DSe-DPEG-DTz, and resulting gelatin-based hydrogels were examined in a HEK-293 cell line by using WST assays. The HEK-293 cells were incubated with several quantities of Gel-Nb, and DSe-DPEG-DTz for 24 h as shown in Fig. 17. Gel-Nb and DSe-DPEG-DTz were compatible against the tested cell line with a maximum concentration of 4000 and 200 μg/mL, respectively. The gelatin hydrogel (GHG-C) also presented good cell compatibility (~100%) as compared to the control. Consequently, the precursors and resulting hydrogels were non-toxic to HEK-293. These results are in accordance with the reported gelatin-derived hydrogels showing less cytoxicities and can be used in medical implants [56], tissue engineering [57], and bone regeneration applications [58].

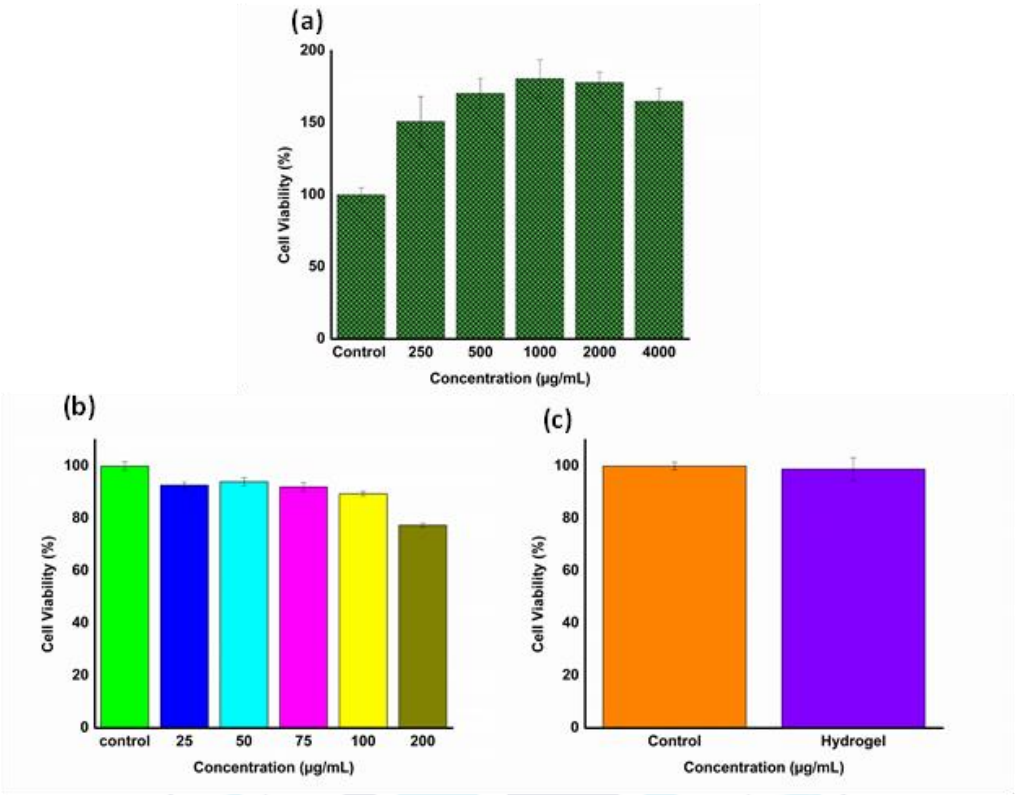

Fig. 17 The in vitro cytocompatibility of precursors and GHG-C tested in HEK-293 cells. (a) Cytocompatibility of Gel-Nb, (b) DSe-DPEG-DTz, and (c) GHG-C hydrogels.

2.6.7. The anti-cancer effect of formulated hydrogels

The *in vitro* anti-cancer activity of the drug-loaded hydrogels (AR3, AR4) was performed using BT-20 cells in the medium with 10 mmol of GSH as shown in Fig. 18a. The cells incubated with the free-DOX molecules showed about 6% cell viability at concentration of 20μg (Fig. 18a). AR3 comprising an equal amount of DOX (20 μg) showed almost similar cell viability (4.6%) by comparing with free-DOX. In contrast, AR4 showed 15% cell viability, which was greater than free DOX. This result can be explained by the fact that less amount of DOX was involved in the cell cytotoxicity due to the strong interaction of ICG and DOX even though the hydrogel network collapsed under the reducing environment [52].

To assess NIR light-induced drug release and associated anti-tumor activity, AR5 was floated in the culture medium of BT-20 cells and exposed to NIR light (2 W, 180 s). The cell viabilities of BT-20 cells incubated with the hydrogels with and without NIR treatment were represented in Fig. 18b. The anti-tumor effect occurred by AR6 without NIR exposure because a small amount of DOX was diffused out to cause the cytotoxicity. In contrast, the anti-tumor activity was greatly pronounced with the exposure of NIR light to the hydrogels, indicating 14% cell viability. The greater anti-tumor activity of these hydrogels with NIR exposure could be ascribed to the burst DOX release due to the breakage of the Se-Se bonds in the hydrogel matrix.

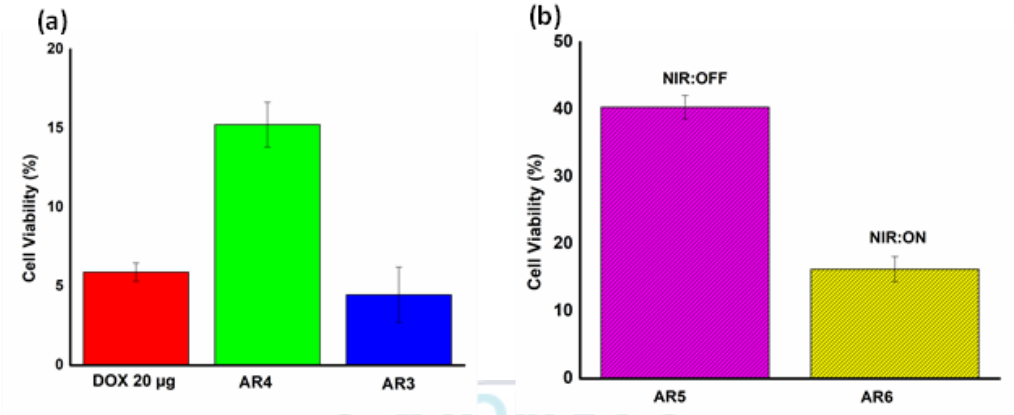

Fig. 18 The cytotoxicity analysis of hydrogels. (a)The effect of the free-DOX, AR3, and AR4 on BT-20 cell viability treated with GSH for 48 h. (b) BT-20 cells viability of AR6 and AR5 after treatment for 48 h under with and without NIR-exposure (2-W power, 180 s).

2.6.8. Fluorescence based live/dead assay

Furthermore, the live dead assay (calcein-AM and ethidium bromide) was conducted to confirm the biocompatibility of BT-20 after the cell viability experiments, as depicted in Fig. 19. The confocal images displayed higher cell viability presented in the form of green color while red color indicated the dead cells. These results presented no substantial difference in live and dead cell count when treated with the control and blank hydrogels, indicating that the blank hydrogels did not exhibit any toxicity in tumor cells. By contrast, AR1 and AR2 showed fewer cell viabilities of BT-20 cells, which proved their antitumor potential against these cell lines.

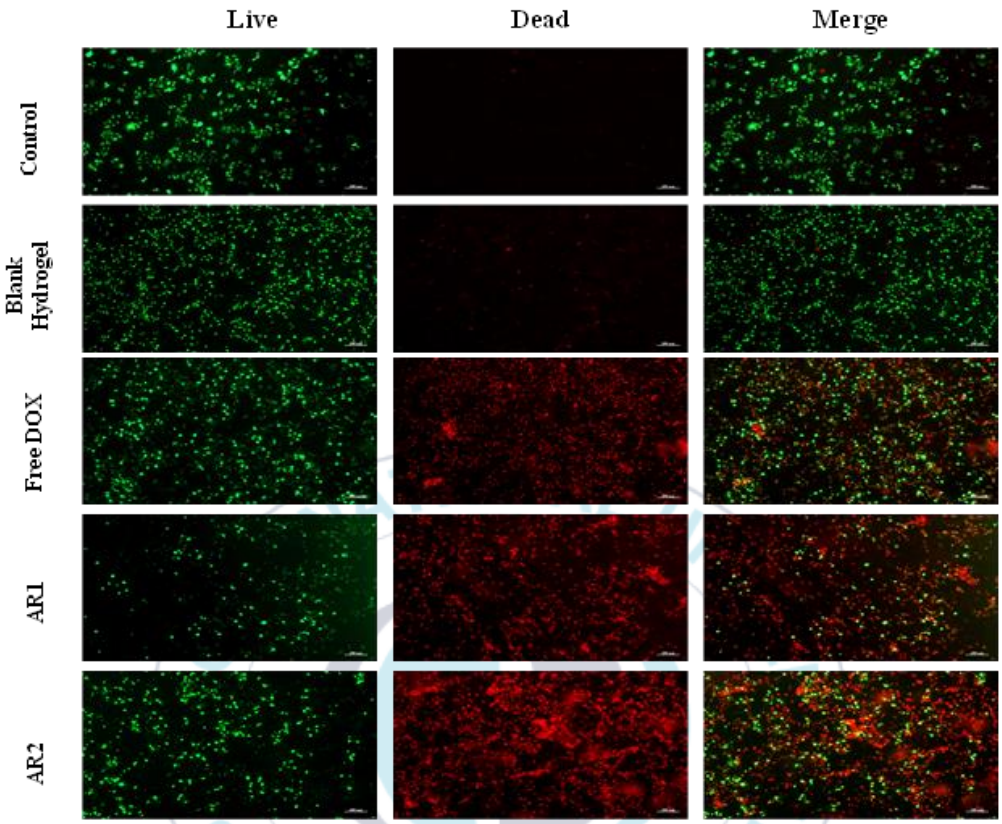

Fig. 19 The confocal laser scanning micrographs depicting the cytocompatibility of free DOX, AR1, AR2 in BT-20 cells. The cell viability was estimated through live/dead assay using calcein-AM/ethidium homodimer-1 fluorescent dyes. Green color indicates the live cells, while red color indicates the dead cells. Visualizing distance 200 μm.

2.6.9. Degradation studies of the hydrogels

The stimuli sensitive drug delivery systems are designed for a specific period of time, releasing the drug molecules at the intended site in a pre-determined tunable fashion [59]. After the liberation of the drug molecules the crosslinked networks needs to be removed from the application site which otherwise would disturb the normal physiological pathways. The biodegradation of the hydrogels plays a key role in removal of these foreign chemical substances from the application site. The results of the degradation analysis of the synthesized hydrogels are shown in Fig. 20. In normal simulated physiological medium i.e., PBS pH 7.4 90% loss in mass was observed after 8 d which could be ascribed to the biodegradation of gelatin backbone responding to the physiological condition. In case of GSH (10 mM), the hydrogels degraded in a time period of 3 d with 85% weight loss showing fast degradation behavior attributed to the GSH induced lysis of the Se-Se bonds [60]. The NIR based hydrogel degradation took a bit longer time then GSH with 90% weight loss in 4 d indicating the indirect cleaving effect of NIR (by decomposing ICG to produce ROS) on Se-Se bonds. The degradation pattern of the hydrogels was correspondent to the DOX release patterns observed as a result of the specific stimuli.

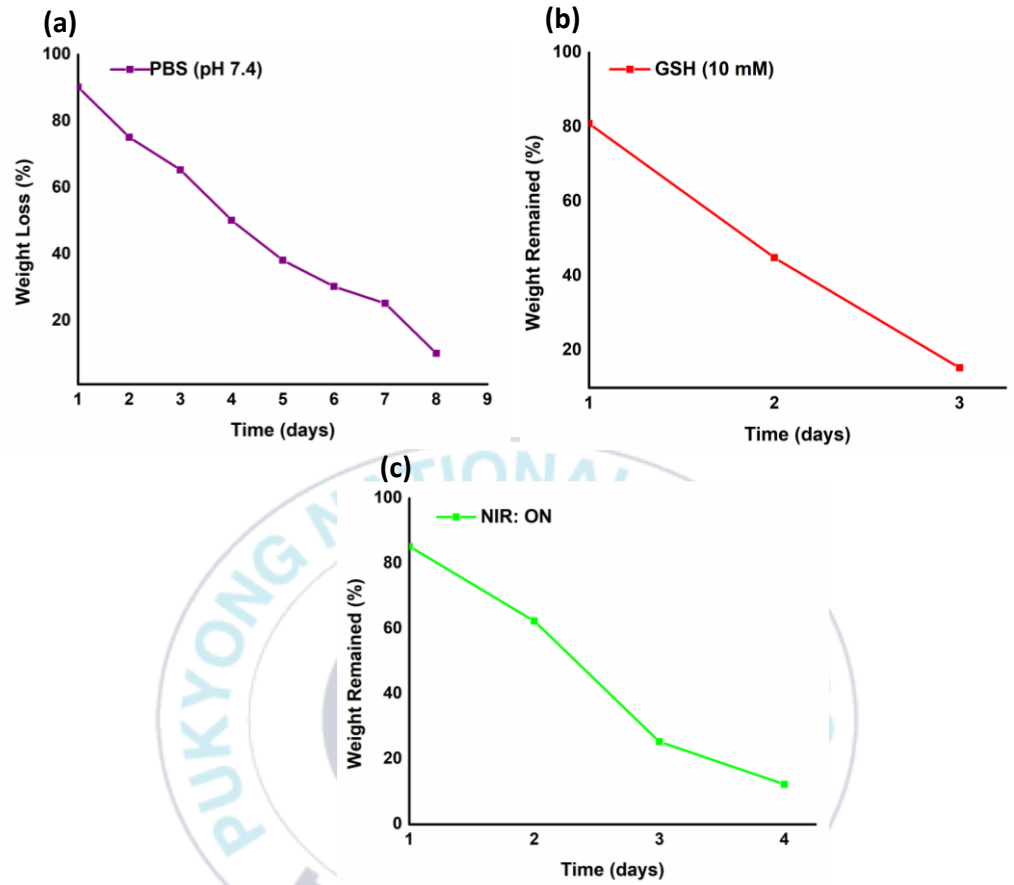

Fig. 20 The degradation analysis of the GHG-C hydrogels in (a) PBS (pH 7.4), (b) GSH (10 mM), and (c) NIR (10 min, 2-Watt, 808 nm).

2.7. Conclusion

Dual responsive gelatin-derived hydrogels were formulated using the diselenide cross-linker through IEDDA "click chemistry" for potential applications in drug delivery systems. Gelatin was first functionalized with Nb moieties and allowed to react with the DSe-DPEG-DTzcross-linker to produce the hydrogels having redox and NIR stimuli responsiveness. The hydrogels with different concentrations of DSe-DPEG-DTzaltered the gelation time (170-523 sec) along with their corresponding swelling ability, release profile, and rheological properties. The hydrogels showed excellent drug loading efficiency and released a nominal amount of DOX (<30%) under physiological conditions. Under GSH environment and NIR irradiation, AR3 and AR4 showed the quick release of the drug initially and later the sustained release up to total amounts of ca. 95 and 82% of the encapsulated DOX for 48 h, respectively. The cytotoxicity data showed that the precursors and the prepared hydrogels were cytocompatible with the HEK-293 cells. The AR1 hydrogels showed similar antitumor efficiency to the free DOX solution. Similarly, AR6 hydrogels also exhibited good anti-tumor activity after NIR exposure. The hydrogels undergone spontaneous biodegradation in all release mediums. Consequently, the gelatin-derived hydrogels can be possibly used as drug carriers with dual (redox and NIR) responsiveness for cancer therapy.

Chapter 3: Facile fabrication of NIR-responsive Alginate/CMC hydrogels derived through IEDDA click chemistry for photothermal-photodynamic anti-tumor therapy

3.1. Introduction

Malignant tumors continue to be one of the major threats to human health closely related with a high mortality and recurrence rate [61]. In order to cure the cancer cells, doxorubicin (DOX) is prominently used for various types of liver, breast [62], and colon tumors [63]. However, cardiotoxicity, the primary side effect of DOX that can occur both acutely and persistently and impact patients' general health, prevents clinical application of DOX [64]. To address this issue, researchers are adopting photothermal/photodynamic (PTT/PDT) strategies for cancer treatment due to its short time, reducing patient suffering and potential therapeutic effects [65]. This technique represents a noninvasive therapy inducing heat by the photothermal agent, such as indocyanine green (ICG), by irradiating near infrared (NIR-808 nm) light leading the generation of reactive oxygen species (ROS) to kill cancer cells [66]. The development of sophisticated delivery systems is essential in the effort to enhance the effectiveness of PTT-PDT. Among these, polysaccharide-derived hydrogels have garnered significant attention owing to their excellent biocompatibility and biodegradability initiating no immune reaction, allowing polysaccharide an ideal candidate for hydrogels scaffold [67]. These biocompatible hydrogels are extensively applied in numerous biomedical areas such as tissue engineering [68], drug delivery [69], 3D bio-printing [70], and wound healing [68] procedures.

Concerning this, naturally occurring polysaccharides such as chitosan, alginate (Alg), guar-gum, hyaluronic acid and carboxymethyl cellulose (CMC) having

extended chains of mono/disaccharide linked by glyosidic bond are thought to be handy biopolymers [71]. Among them, Alg has been utilized as a cheap source of biomaterials extracted from seaweed owing to the successive distribution of α-L-guluronic acid and β-D-mannuronic acid with excellent biocompatibility and gel-forming properties [28]. On the other hand, CMC which possesses high hydrophilicity, low viscosity and facile modification capability makes it a suitable candidate for developing biocompatible hydrogels [72]. Combining these two biopolymers, Alg/CMC, offers a unique opportunity to exploit their synergistic properties for the development of hydrogels for PTT-PDT applications.

A major obstacle in creating hydrogels from polysaccharides was regarded to be the requirement for an effective and facile fabrication method. Historically, Alg has been cross-linked using ionic cross-linking, which resulted in poor mechanical properties, thus limiting its capacity to load drugs [73-75]. Utilizing the -COOH functional group within the Alg polymer chains simplified the process of functionalizing Alg. As a result, a wide range of covalent cross-linking methods, such as the thiol-ene reaction, [76] azide alkyne cycloaddition [77] and photochemical cross-linking [78] could be used for development of hydrogel systems. Although these approaches were simpler and more practical but the majority of them contained hazardous chemicals and catalysts that could have a detrimental impact on associated biopolymers. Hence, there is a need for methodologies that have reduced adverse effects when working with polysaccharide-derived hydrogels. Recently, "click" reactions have emerged as a successful alternative approach to produce Alg hydrogels with minimal toxicity [35]. The inverse electron-demand Diels-Alder reaction (IEDDA) reaction provided a high degree of chemo-selectivity and boasted an exceptionally rapid reaction rate under mild conditions. Furthermore, it

generated N_2 gas as a by-product, which could serve as a pore-forming agent [44]. Hydrogels featuring porous structures could offer added benefits when it comes to drug loading and release characteristics. However, the majority of the techniques described in the literature have utilized harmful co-solvents such as DMSO in the fabrication process of hydrogel networks, potentially compromising their biocompatibility [44].

When designing therapeutic carriers for controlled drug release, another crucial factor to consider is the responsiveness of the polymeric hydrogels to external stimuli. These stimulus-responsive hydrogel systems can be triggered by various external stimuli, including pH, temperature, redox reactions, near-infrared (NIR) light, ultrasound, and magnetic fields. Among these stimuli, NIR-light is considered safer for cells due to its low radiation energy (in the range of 650-900 nm) and its ability to penetrate tissues effectively, thereby inducing a biochemical response [79]. Our research group has incorporated ICG, a photosensitizer and NIR responsive dye, into polysaccharide-derived hydrogels for NIR responsive drug delivery application [80]. ICG possesses the capability to generate ROS through the absorption of near-infrared (NIR) irradiation at 808 nm [81]. ROS could stimulate the degradation of hydrogels and on-demand release of therapeutic agents in a controlled manner. On the other hand, ROS itself can be useful for PDT [82] . It is also known that NIR absorption to ICG generates heat as well as ROS, which utilized to PTT [83].

In our current research, we have designed a facile hydrogel system having the ability to produce ROS. The injectable CMC/Alg hydrogel was depicted in Scheme 3, based on the IEDDA click cross-linking reaction between Alg-methyl tetrazine (Alg-mTz) and CMC-norbornene (CMC-Nb). ICG was incorporated during the formation of hydrogels, which could produce ROS with elevation in temperature upon NIR irradiation. In the cell line under investigation, CMC-Nb,

Alg-mTz, and the fabricated hydrogels displayed no cytotoxic effects. Contrary to this, the ICG-loaded hydrogels showed anti-tumor properties against the HeLa cell line and inhibited the explosion of HeLa tumor cells following exposure to NIR light.

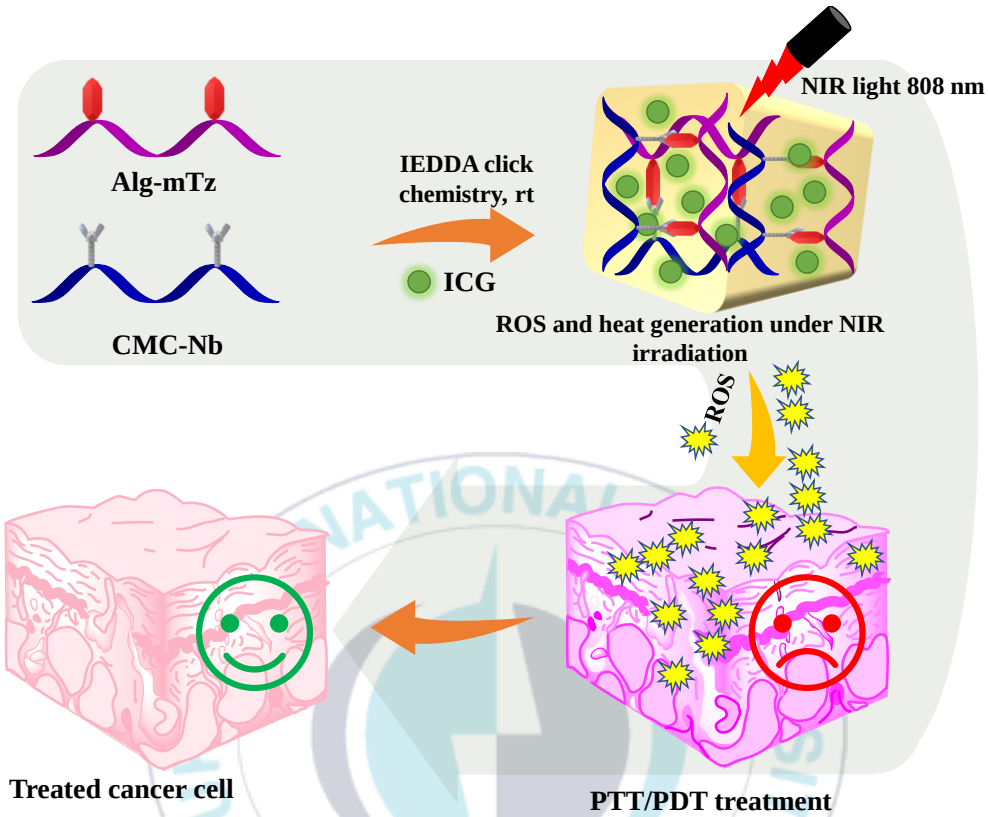

Scheme 3 The schematic of polymer/polymer-derived hydrogel and the mechanistic pathway for ROS generation under irradiation of NIR laser (808 nm).

3.2. Experimental

3.2.1. Materials

Sodium alginate (Mw = 120-190 kDa), CMC (M_W ~ 276 kDa), 5-norbornene 2-methylamine, 1-ethyl-3-(3-dimethylaminopropyl)-carbodiimide hydrochloride (EDC. HCl, 99 %), and ICG were procured from Tokyo Chemical Industries (TCI, Japan). Methyl tetrazine amine HCl salt was purchased from Conju-Probe, LLC, USA. N-hydroxysuccinamide (NHS 98 %) was acquired from Sigma Aldrich. All other reagents were of analytical quality and used without further processing.

3.2.2. Instruments

The analysis of ^{1}H-NMR spectra was conducted with a NMR instrument, specifically the JNM ECZ-400 model from JEOL. An Agilent CARY 640 spectrometer was used to acquire FTIR spectra. The surface and internal structures of CMC/Alghydrogels were examined by means of field emission scanning electron microscopy (FE-SEM, MIRA 3 system TESCAN). A UV-Vis spectrophotometer (Optizen POP, Optizen) was utilized to measure UV-Vis spectra in the range of 400-800 cm^{-1}. The mechanical properties of the scaffolds were assessed using a hybrid rheometer (DHR-2, TA-instrument).

3.3. Polymer conjugation for the development of hydrogels.

3.3.1. Coupling of Alg with Methyl Tetrazine Amine

Alg-mTz was synthesized following the previously established protocol with minor adjustments, as illustrated in Scheme 4A [84]. Firstly, 1000 mg of sodium alginate (0.0065 mmol) was dissolved in 100 mL of deionized (DI) H2O overnight to make a homogenous solution. EDC. HCl (193 mg, 1.005 mmol)

and NHS (174 mg, 1.508 mmol) pre-dissolved in DI H2O and DMSO respectively, were added into the Alg solution and allowed to react for one hour. Afterward, mTz (239 mg, 1.006 mmol) pre-dissolved in DMSO (2 mL) was introduced slowly into the reaction vessel. The solution was agitated for 24 h at room temperature (RT). An excessive amount of acetone (3 × 100 mL) was added to quench the reaction, resulting in the formation of a pink-colored solid product. The product was dried and re-dissolved in DI water. Then the product was continuously dialyzed through dialysis tubing (MWCO = 14 kDa) for 72 h. Finally, the conjugated material underwent a 48-h freeze-drying process, leading to Alg–mTz with a good yield (65%). The conjugation of Alg with mTz was clarified through 1H-NMR spectroscopic analysis.

3.3.2 Conjugation of CMC with Norbornene Amine

CMC underwent chemical modification with a norbornene moiety via an amidation process using an EDC coupling reaction, in line with the previously published work [72]. The process, as depicted in Scheme 2B, commenced with the dissolution of 1000 mg of Na–CMC (0.0036 mmol) in 100 mL of DI H2O at RT overnight, resulting in a homogenous solution (1% w/w). In the subsequent step, EDC. HCl (580 mg, 3.04 mmol) and NHS (340 mg, 3.04 mmol) were introduced into the CMC solution to activate the COOH functional groups along the CMC backbone. The reaction was stirred at RT for 2 h. After completing the activation step, 370 µL (3.04 mmol) of 5-norbornene-2-methylamine was added incrementally to the reaction mixture, which was then stirred at RT for 24 h. The product was precipitated by employing 3 × 100 mL acetone. The resulting white fluffy product was obtained through vacuum filtration and subsequently dried in a vacuum oven. The product was then re-dissolved in deionized water to attain a 1% concentration (w/v) and subjected

to dialysis using a 14 kDa MWCO membrane tubing for 72 h. The final yield of CMC with norbornene (CMC–Nb), which surpassed 80%, was achieved through lyophilization. The confirmation of CMC modification with norbornene amine was verified using 1H-NMR spectroscopy.

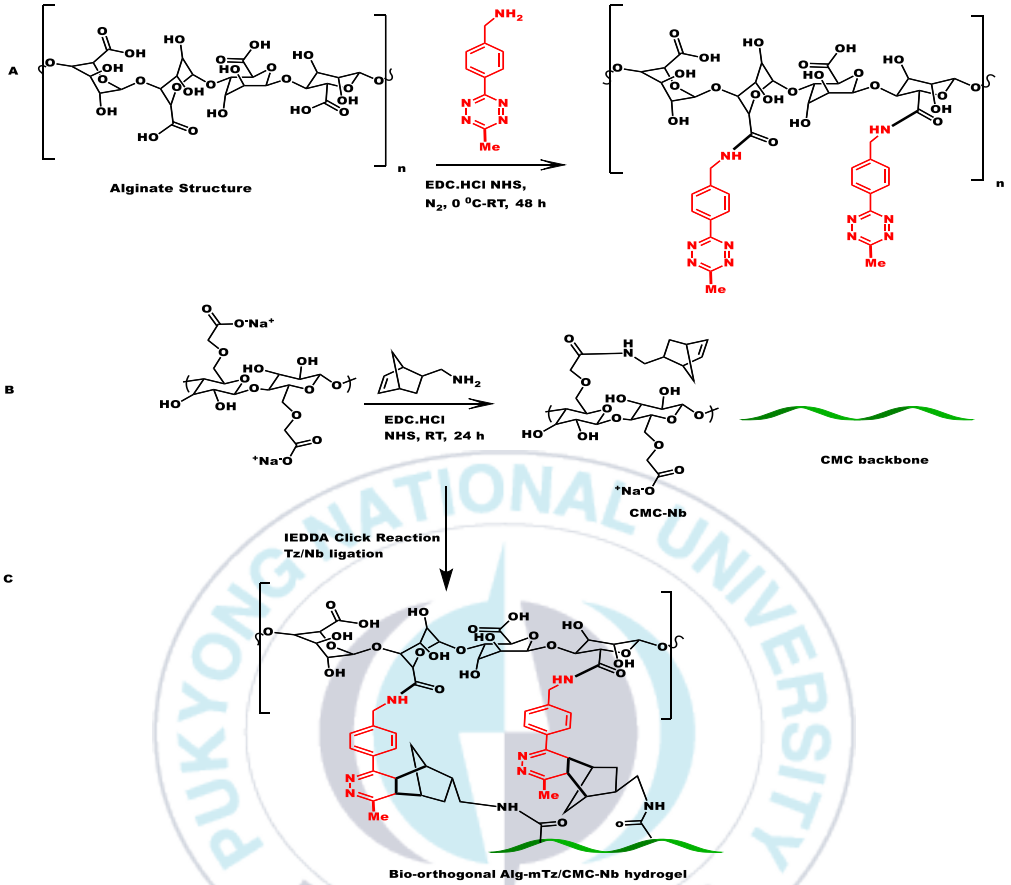

Scheme 4 The synthetic route path for polymer-polymer conjugation, (A) bio-conjugation of alginate with methyl tetrazine amine, (B) Functionalization of CMC with norbornene amine, and (C) formation of polymer-polymer derived click hydrogel.

3.4. Hydrogel fabrication

To prepare CMC/Alg-based hydrogels, a vial was charged with 200 µL of CMC–Nb (2.5% w/v) in DI water and subjected to stirring until a uniform solution was achieved. Simultaneously, two weight % ratios of Alg–mTz (200 µL) (as shown in Table 1) were dis-solved in DI water, contingent upon different molar ratios of Nb/Tz (1:1.70 and 1/0.85). Both CMC–Nb and Alg–mTz solutions were mixed and subjected to vortexing for 20 sec to promote the formation of a homogeneous phase, facilitating hydrogel fabrication as depicted in Scheme 4C.

Table 4 Molar feed ratio of polymer-polymer hydrogels.

Sr. No.	Hydrogel Code	CMC-Nb:Alg-mTz (% w/v)	Nb:Tz mmol
1	CA-1	2.5:2.5	1:1.70
2	CA-2	2.5:1.25	1:0.85

3.5. Characterization

3.5.1. Rheological Analyses of CMC-Alg hydrogels

The mechanical properties of CMC/Alg-based hydrogels were carried out by dynamic oscillation of two parallel plates to determine the storage (G′) and loss (G″) moduli respectively. In the frequency sweep test, a constant strain (1 %) was applied with varying the angular frequency from 0-100 rad/s, while the dynamic oscillatory strain amplitude sweep experiments were measured with the applied strain range (0.1 to 10,000 %) keeping the angular frequency constant at 10 rad/s.

3.5.2. Swelling Properties

The ability of hydrogels to swell was evaluated using a gravimetric approach. Lyophilized hydrogels were placed in a sufficient quantity of pH 7.4 PBS solution at physiological temperature. The weight of the swollen hydrogels was measured at specific time intervals until a stable weight was reached. This experiment was repeated three times for each hydrogel. The equilibrium swelling ratio (ESR) was calculated using the following equation.

$$ESR\ \% = (Ms - Md/Md) \times 100 \quad (6)$$

In the equation, "Ms" represents the mass of the swollen hydrogels, and "Md" represents the mass of the lyophilized hydrogels.

3.5.3. The structural characteristics of CMC/Alg hydrogels

FE-SEM was employed to examine the surface and interior structures of the fabricated hydrogels. Prior to analysis, the hydrogel samples were lyophilized and vertically sliced in liquid nitrogen.

3.5.4. *In vitro* ROS generation

The in vitro ROS generation ability of hydrogels (CA-1) was assessed by using 1,3-diphenylisobenzofuran (DPBF) assays. To conduct the experiment, 10 µL of a DPBF solution (3.7 mmol., in DMSO) was introduced into a quartz cuvette containing CMC/Alg hydrogels loaded with 20 µg of ICG. NIR light exposure was performed for 5–15 min at power levels of 1 W and/or 2 W. The fluorescent intensities of the samples were measured in the wavelength range of 420–700 nm, with excitation at 410 nm.

3.5.5. *In vitro* cytocompatibility analysis of the precursors and hydrogels

The cytocompatibility of CMC–Nb, Alg–mTz, and CMC/Alg hydrogels was evaluated using the WST assay (EZ-cytox, South Korea) with human embryonic kidney cell line (HEK-293). The cells were cultured in DMEM supplemented with 10% fetal bovine serum (FBS) and 1% antibiotic–antimycotic solution in an incubator at 37 °C with 5% CO2 for 24 h, then seeded in a 48-well plate at a density of 10^4 cells per well. Subsequently, the culture medium was aspirated and replaced with a fresh culture medium containing CMC–Nb (125–2000 µg/mL) and Alg–mTz (125–2000 µg/mL). After 24 h, the cells were rinsed twice with PBS (100 µL). Next, a fresh medium with the WST assay solution (10 µL) was added to each well. Cell viability was determined by measuring the optical density at a wave-length of 450 nm using a microplate reader.

3.5.6. Fluorescence-based live/dead assay

Cellular viability and cell death assays for both blank hydrogels and CA-1 (equivalent to 20 µg of ICG) were conducted on HEK-293 cells. After the treatments mentioned above, the cells were stained with calcein-AM to distinguish viable cells (appearing green) and then further stained with ethidium

bromide to detect non-viable cells (appearing red) using a fluorescence microscopy technique.

3.5.7. *In Vitro* Photothermal Effect and Photothermal Conversion Efficiency of Hydrogels

The photothermal test consisted of exposing free PBS, free ICG (1 mg/mL in PBS), and the ICG-loaded hydrogel (CA-1) to NIR laser irradiation, with power settings at both 2 W/cm^2 and 1 W/cm^2 for a duration of 10 min. Temperature fluctuations in the samples were monitored using a thermometer every minute over the course of 10 min.

The photothermal conversion efficiency η of Alg/CMC hydrogels was calculated ac-cording to the following equations:

$$\eta = \frac{hA(T_{max}\text{-}T_{surr})\text{-}Q_{Dis}}{I\left(1\text{-}10^{-A\lambda}\right)} \quad (7)$$

$$Q_{Dis} = h_0 A(T_{max} - T_{surr}) \quad (8)$$

where h is heat transfer coefficient, A is surface area of the container, T_{surr} is the ambient temperature, T_{max} is the highest temperature of the sample under NIR irradiation 808 nm laser, I is the power density of laser (2 W/cm2), A_λ is the is the absorbance of ICG at 808 nm, and Q_{Dis} is the heat loss of the light absorbed the quartz sample cell [85].

3.5.8. Anti-cancer effect of the ICG-loaded hydrogels

The anti-cancer potential of the ICG-entrapped hydrogels was evaluated using a WST assay with a HeLA cell line. The cells were cultured and seeded in a 48-well plate. The existing culture medium was replaced with a fresh medium containing PBS (pH 7.4). Subsequently, the cells were exposed to CA-1 (by placing hydrogels on the cell culture medium) for 48 h, followed by treatment with NIR irradiation (808 nm, 3 min, 2-W power).

3.5.9. Statistical analysis

All physiochemical investigations were conducted in triplicate, while cell culture as-says were performed with four replicates. The data are presented as the mean ± standard deviation the student's t-test was used to evaluate the significance. The statistically significant ($p < 0.05$) and very significant ($p < 0.001$) were used to consider the difference be-tween two results.

3.6. Results and Discussion

3.6.1. Synthesis of CMC-Nb

The synthesis of CMC-Nb was carried out with 5-norbornene-2-methyl amine and CMC by the EDC/NHS coupling reaction (Scheme 4B). The conjugated CMC was purified by acetone followed by dialyzes against 14 KDa membrane using DI water. The norbornene functional moieties provided reactive sites for mTz counter groups located at the backbone of Alg polymer to perform an IEDDA click reaction for the formulation of CMC-Alg hydrogels. The ^{1}H-NMR spectrum verified the incorporation of Nb into the CMC backbone, as illustrated in Fig. 21a. The double bond signals of the Nb groups were observed in the 5.9-6.2 ppm range, while the region between 3.2-4.5 ppm corresponded to the CMC backbone [86]. The degree of substitution (DS), which was calculated to be 7.7%, was determined by integrating the protons associated with Nb and the CMC backbone.

3.6.2. Coupling of Alg with methyl tetrazine amine

Alg was conjugated by mTz using the EDC/NHS coupling mechanism through which carboxylic functional groups of the Alg molecule were allowed to react with methyl tetrazine amine to form Alg-mTz presented in Scheme 4A. The modification of Alg with mTz, as depicted in Fig. 21b, was verified through the ^{1}H-NMR spectrum. The peaks appeared at 7.5 and 8.5 corresponding to the benzene ring proton of the tetrazine ring, which is evidence of the conjugation of Alg with methyl tetrazine amine [87]. DS was determined to be 3.2%, calculated by the ratio of protons from the benzene ring to the backbone of the Alg molecule.

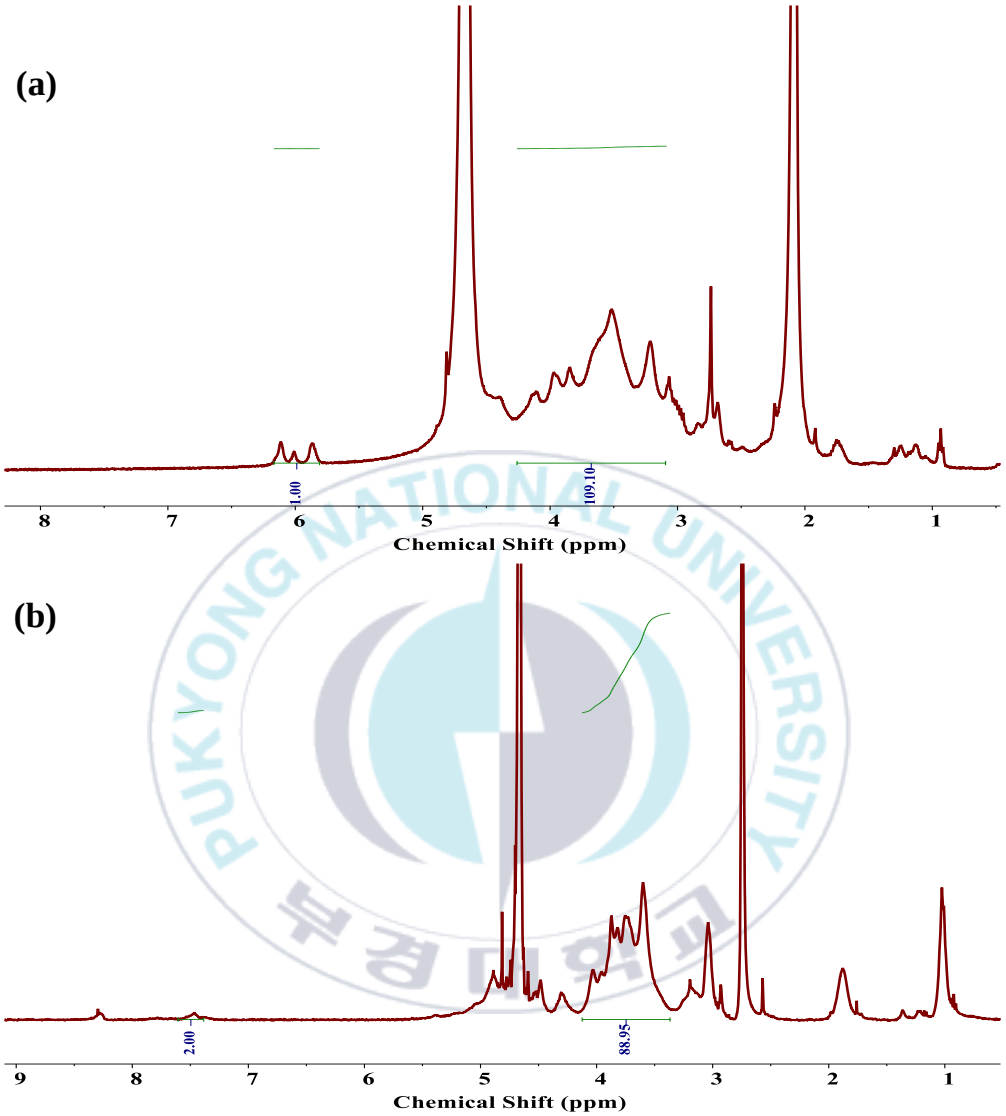

Fig. 21 ^{1}H-NMR spectra of the precursors. (a) CMC-Nb and (b) Alg-mTz

3.6.3. Preparation and mechanical properties of CMC/Alg-derived hydrogels

Two different kinds (CA-1 and CA-2) of CMC/Alg-derived hydrogels were fabricated with varying Nb/Tz molar feed ratios (Table 4). After agitating the precursor solutions by using a vortex mixer, the Nb and mTz moieties were engaged in an IEDDA click reaction that produced CMC/Alg-derived hydrogels. The optical images of fabricated hydrogels were shown in Fig. 22. The interaction between the Nb and mTz groups was confirmed by analyzing the FT-IR spectra of the hydrogel samples.

The FT-IR spectra (Fig. 23) displayed the characteristic alkene bond peak (C = C) of mTz at 1631 cm^{-1}, indicating the successful introduction of mTz moieties through the IEDDA click reaction. The C-H peak of the methyl group which appeared at 1397 cm^{-1} gave indication of the methyl ($-CH_3$) attached to the benzene ring of the tetrazine moiety. According to the molar concentrations of Alg-mTz in the reaction formulation, the hydrogels were assigned to CA-1 and CA-2. The concentration of the Alg-mTz solution could alter the cross-linking density. The rapid IEDDA click reaction resulted in effective conversion without the need for a catalyst [88].

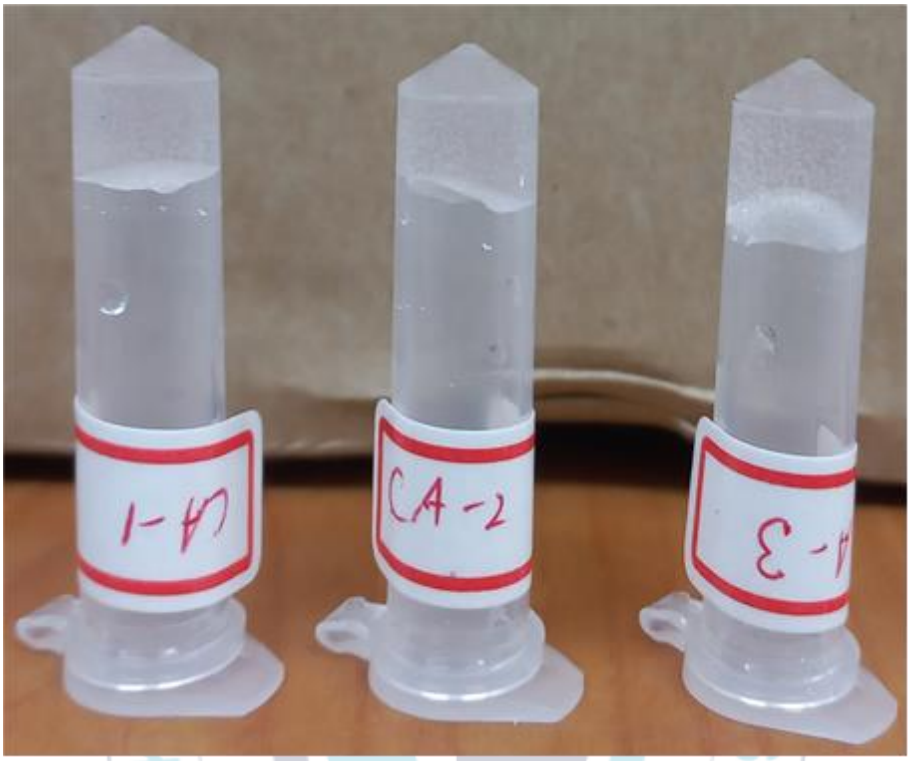

Fig. 22 Photographic images of fabricated hydrogels derived from bio-conjugated polysaccharide.

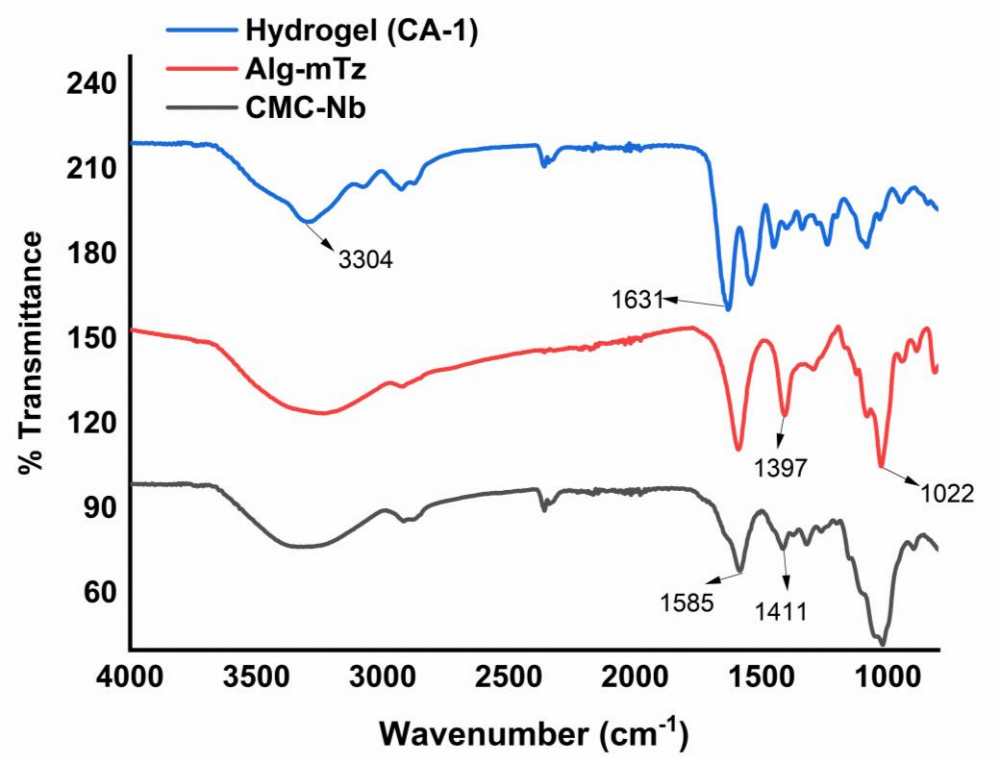

Fig. 23 FT-IR spectrum of CMC-Nb, Alg-mTz and formulated hydrogel.

The rheological characteristics of hydrogels are crucial for drug delivery applications [89]. We measured the mechanical robustness of the CMC/Alg-derived hydrogels by computing the storage/loss modulus (G′/G″). The acquired values were subsequently graphed against angular frequency, as shown in Fig. 24a-b.

In the frequency sweep analyses, G′ consistently exhibited higher values than G″, elucidating the flexible nature of the fabricated hydrogels. It could be observed that the G′ of hydrogels increased as the feed ratios of the tetrazine counterpart increased (which resulted in higher cross-linking density). The storage modulus values at the initial frequency of the hydrogels (CA-1 and CA-2) were measured as 492 and 270 Pa, as depicted in Fig. 24a-b, respectively. These outcomes show that the mechanical robustness of hydrogels has a direct relation with the extent of cross-linking as described previously [90]. The viscoelastic nature of the hydrogels was further investigated by analyzing dynamic oscillatory strain amplitude-sweep tests. Precisely, the study was conducted to confirm the linear viscoelastic region (LVR) of hydrogels as presented in Fig. 24c.

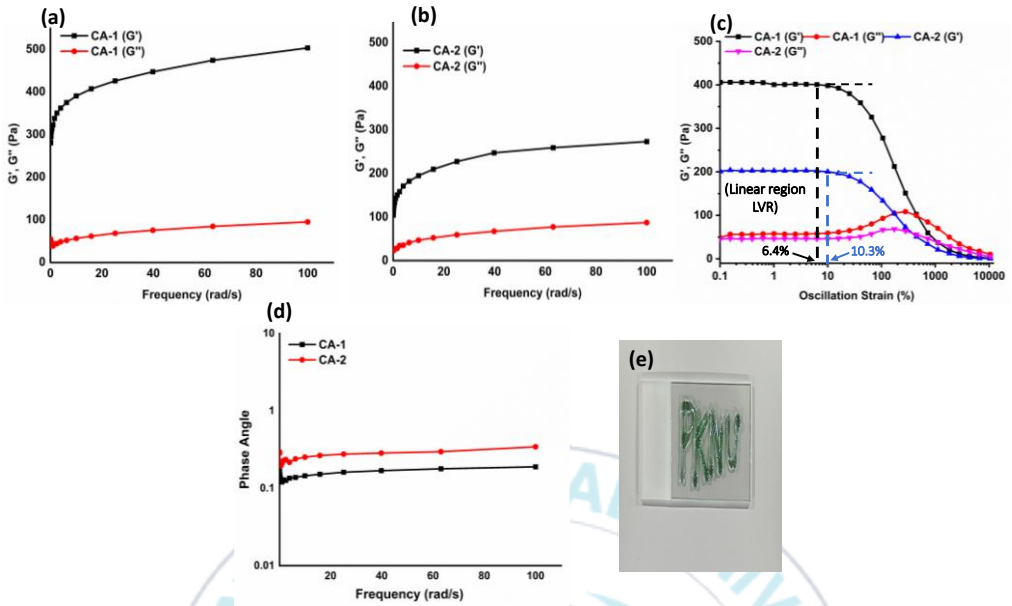

Fig. 24 The viscoelastic characteristics of the hydrogels, with (a-b) representing the moduli as a function of angular frequency of CA-1 and CA-2 hydrogels, respectively, (c) the strain amplitude sweep experiment, (d) phase angle as a function of angular frequency, (e) photographs of injectable hydrogel loaded with ICG.

The viscoelastic behavior of hydrogels, characterized by their G' and G" values, remains relatively consistent regardless of the level of applied strain. The hydrogels CA-1 and CA-2 exhibited LVR within the respective ranges of 0.1-6.4% and 0.1-10.3% respectively, demonstrating the sufficient cross-linking leads to the decreased value in LVR of hydrogels.

It is also reported in the literature that LVR steadily decreases as hydrogel turns into a solid phase [91]. The critical strain (γc%), which can be defined as the point at which G' values deviate by more than 5% from the plateau values, is a key parameter for hydrogels [92]. The critical strains were observed at various strain amplitudes (15% and 25%), for CA-1 and CA-2, respectively. Beyond the γc%, the values of G′ gradually diminish, indicating the transition of hydrogels from a semi-solid state to a semi-liquid state. Additionally, the phase angle (<1) of hydrogels was assessed across an angular frequency (0.1-100 rad/s), indicating that hydrogels were elastic [93] as presented in Fig. 24d. The injectability of the hydrogels was evaluated by passing CA-1 through a 25-gauge needle, as shown in Fig. 24e, which confirmed that the hydrogels could be precisely delivered into deteriorated tissues or organs.

3.6.4. Swelling performance of hydrogels

The swelling ratio of hydrogels has a considerable impact on drug loading efficiency. The swelling characteristics of the hydrogels were assessed using a gravimetric approach. The equilibrium swelling behavior is presented in Fig. 25, which demonstrates that hydrogel CA-1 and CA-2 swell dynamically during the initial 4 h, indicating a 12, and 40 times rise in mass as in comparison to their original mass, respectively. The hydrogels gradually captivated water during the initial period of swelling and essentially attained their swelling equilibrium by 24 h. The CMC/Alg-derived hydrogels showed higher swelling behavior than Alg/PEG-derived hydrogels in the previous report [28].

Interestingly, both the carbohydrate polymers have COOH functional groups at their respective backbones rendering the higher ESR. At a pH of 7.4, the Alg and CMC chains experience deprotonation, resulting in the formation of negatively charged $–COO^{-1}$ anions. This process leads to the creation of repulsive forces within the polymer networks. These anionic groups could induce more hydrophilicity and hydrogel networks expanded more effectively [94]. The results suggest that the CMC/Alg-derived hydrogels will be beneficial for drug delivery application due to the higher swelling properties.

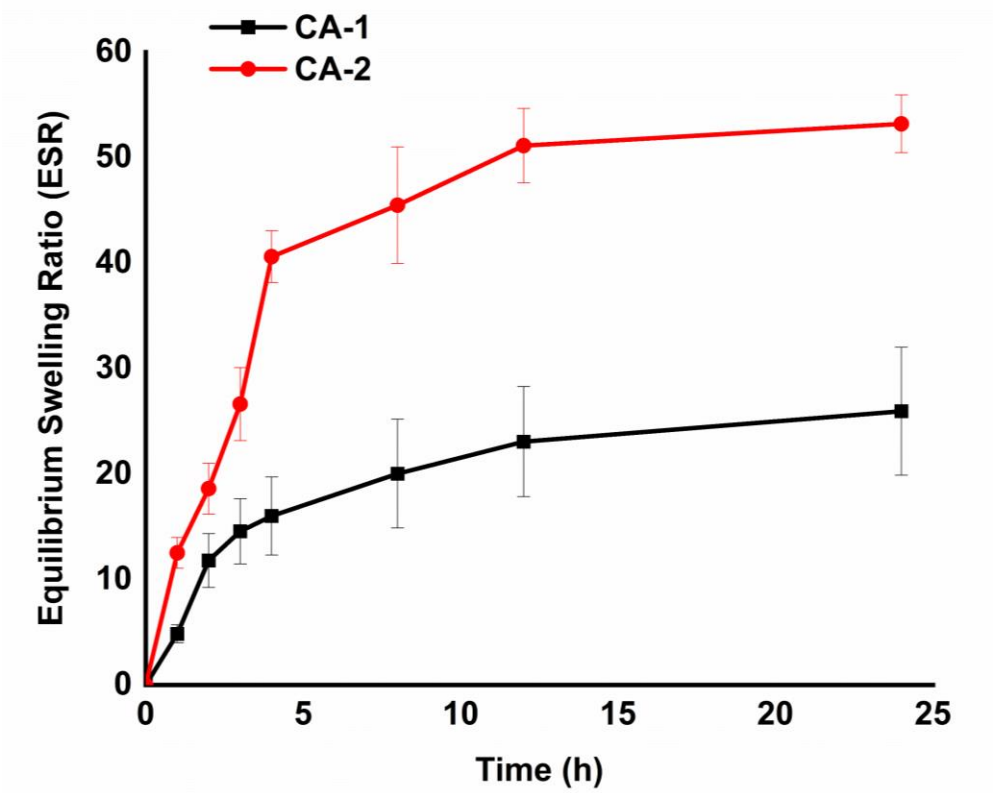

Fig. 25 Equilibrium swelling capability of hydrogels in PBS (7.4)

3.6.5. Morphology of hydrogels

The CMC/Alg-derived hydrogels exhibited porous morphologies, which have the potential to provide advantages in various biological applications, including drug delivery and tissue engineering. The highly porous morphologies observed in the injectable hydrogels could be attributed to the *in-situ* formation of micro-bubbles within the networks induced by the generation of N_2 gas during the IEDDA click reaction [44,72]. Indeed, the IEDDA click reaction, involving the interaction between methyl-tetrazine (diene: electron-deficient species) and Nb (dienophile: electron-rich species), demonstrated high efficacy under physiological conditions. This reaction resulted in the formation of covalent cross-linking bonds and the release of N_2 gas as a by-product. The porous morphologies of the hydrogels were visualized using FE-SEM after they underwent lyophilization. It is notable that more and smaller holes are observed on the surface of the hydrogels at the higher molar concentration of Alg-mTz (see Fig. 26a and b).

This phenomenon can be attributed to that a greater number of small bubbles were formed in the denser network resulted from the higher IEDDA cross-linking reaction. Meanwhile, the internal structure of all the formulated hydrogels exhibited a high level of porosity, as depicted in Fig. 26c-d. Well-connected pores are evident within the hydrogel system when a higher molar feed ratio of Alg–mTz is employed (see Fig. 26c). In comparison, more open pores are observed with the lower molar feed ratio of Alg–mTz, as illustrated in Fig. 26d. Porosity in injectable CMC/Alg-based hydrogels may play a crucial role in processes such as swelling, drug release, and efficient oxygen supply within the 3D microenvironment.

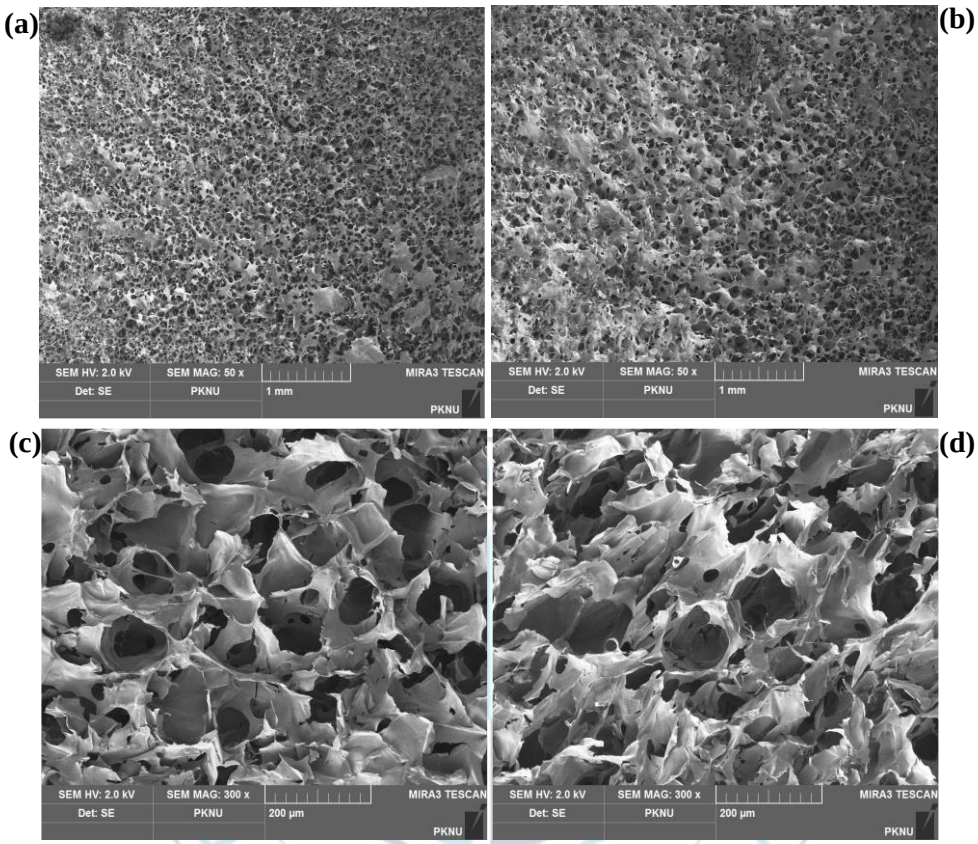

Fig. 26 FE-SEM images of surface morphology (a-b) and cross-sectional area (c-d) of CA-1and CA-2 hydrogels respectively.

3.6.6. *In vitro* ROS detection and photodynamic effect

The production of ROS resulting from the interaction between NIR light and the ICG molecule was evaluated using DPBF as a probe. DPBF is a fluorescent molecule that exhibits a highly specific reaction with ROS, including singlet oxygen and radicals such as hydroxy, alkoxy, alkyloxy, and alkylperoxy. When exposed to ROS, DPBF undergoes rapid oxidation, leading to the formation of 1,2-dibenzoylbenzene or o-benzoylbenzophenone, which results in a decrease in the fluorescence intensity of DPBF. The fluorescence intensities exhibited consistent changes in correlation with both the duration of irradiation (5–15 min) and the power density of NIR light (1–2 W/cm^2).

The ICG-loaded hydrogels (CA-1) exhibited its maximum fluorescence intensity when exposed to 1-W NIR light for a duration of 5 min. Whereas, a significant reduction in fluorescence intensities was observed when subjecting the hydrogel to NIR radiation with the higher power density, as illustrated in Fig. 27a. The DPBF fluorescent intensities was also reduced with prolonged irradiation time (10-15 min), as depicted in Fig. 27b. The porous structure of the CMC/Alg-derived hydrogels might play a crucial role in contributing to their high photothermal and photodynamic performance. The higher porosity facilitates multiple light scattering and reflection, leading to enhanced capture of the incident light and, consequently, improved light absorption [95].

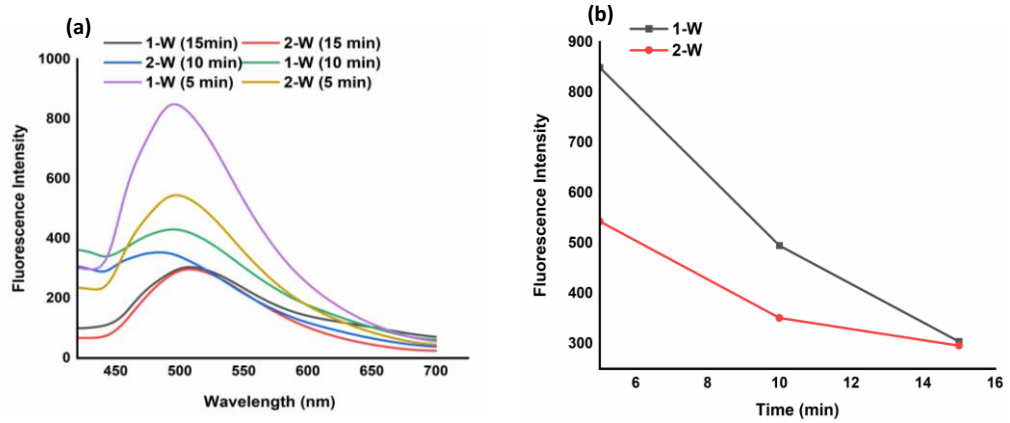

Fig. 27 Photodynamic performance of formulated hydrogels (a) change in fluorescence intensities of DPBF as a function of ROS production under 1-2 W power NIR light for 5-15 min (b) The degradation of DPBF with CA-1 hydrogel at 1-2 W NIR irradiation.

3.6.7. Cytocompatibility analysis

The assessment of cytocompatibility is a crucial factor when considering hydrogels that could potentially impart harmful effects on biological processes. In this context, an *in vitro* examination of the cytotoxicity of CMC-Nb and Alg-mTz was conducted using HEK-293 cells, employing the WST assay. To assess cytotoxicity, HEK-293 cells were subjected to varying concentrations of CMC-Nb and Alg-mTz for a duration of 24 h, after which cell viability was ascertained under controlled light conditions.

The results of the cytotoxicity assessments revealed that the presence of CMC-Nb and Alg-mTz did not exert a significant impact on the proliferation of HEK-293 cells. Notably, CMC-Nb exhibited remarkable biocompatibility and bio-safety, even at the highest concentration tested, which was 2000 μg/mL, with a striking 98% cell viability, as presented in Fig. 28a. These findings highlight the concept that the inclusion of Nb moieties within the structure of CMC does not detrimentally affect its biocompatibility, thereby establishing CMC-Nb as a suitable precursor for the production of bio-orthogonal hydrogels [72]. Similarly, Alg-mTz displayed cell viabilities reaching approximately 80% following exposure to HEK-293 cells at the maximal concentration of 2000 μg/mL, as depicted in Fig. 28b. This observation further highlights the biocompatibility of these precursor materials, which not only permits effective cell proliferation but also demonstrate cell viability levels comparable to those of control groups, thereby affirming their suitability for downstream applications.

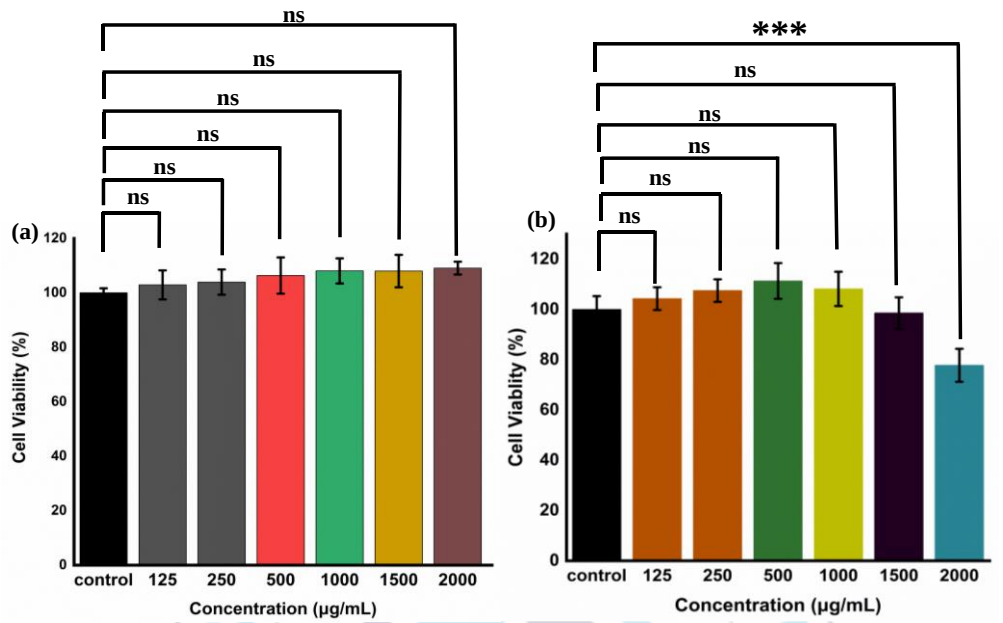

Fig. 28 The In vitro cytocompatibility of precursors in tested HEK-293 cells. (a) cytocompatibility of CMC-Nb and (b) cytocompatibility of Alg-mTz.

3.6.8. Live/dead assay

The live/dead assay, utilizing calcein-AM and ethidium bromide, was carried out to confirm further the biocompatibility of the precursors. In the confocal images, viable cells were prominently displayed in green, while deceased cells were marked in red (see Fig. 29). These findings revealed that there was no significant variance in the count of live and dead cells when exposed to the control, CMC–Nb, and Alg–mTz.

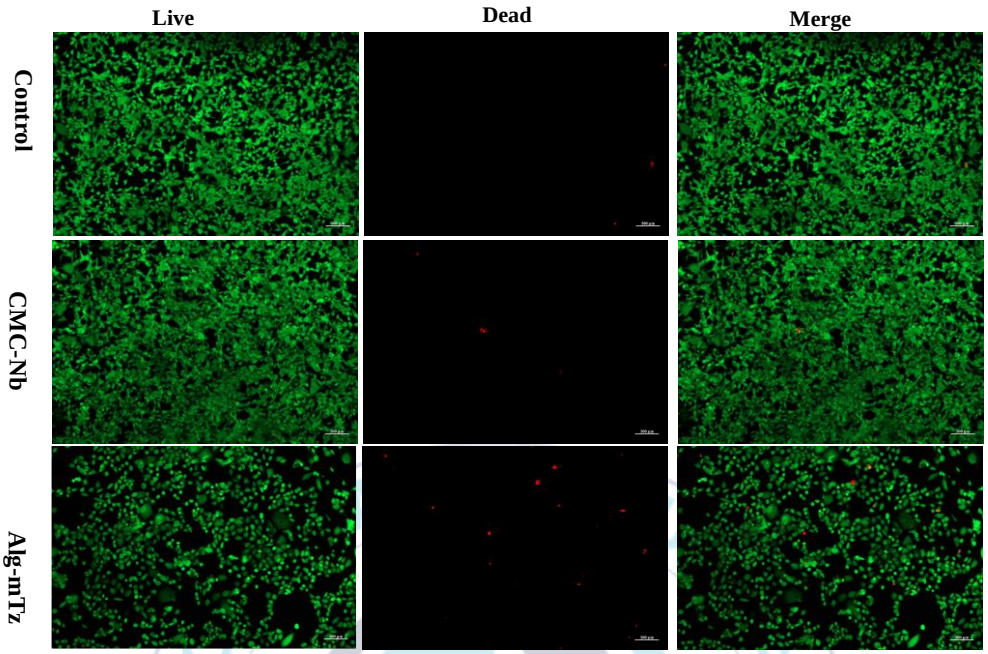

Fig. 29 Confocal laser scanning micrographs showing cytocompatibility of control media, CMC–Nb, and Alg–mTz in HEK-293 cells. Cell viabilities were determined by calcein-AM/ethidium homodimer-1 assay (live/dead assay) Green color represents live cells, whereas, red color represents dead cells. Scale bars showing 100 μm.

3.6.9.The Photothermal Effect under NIR Irradiation and Photothermal Conversion Efficiency of Hydrogels

To assess the potential for hyperthermia induction, NIR laser light was employed to measure temperature elevations (ΔT) in both the CMC/Alg-derived hydrogels and their respective solutions. As the duration of NIR light exposure increased incrementally from 0 to 10 minutes, a corresponding temperature rise was observed, reflecting also the increased power of the NIR light source (Fig. 30).

An examination of thermal images (Fig. 31) revealed that hydrogel CA-1 and the free PBS solution exhibited negligible temperature fluctuations following 10 min of laser irradiation. In contrast, free ICG and ICG-loaded hydrogels exhibited substantial temperature variations in direct correlation with the increasing intensity of the laser irradiation. It is worth noting that there exists a directly proportional relationship between laser intensity and the resulting temperature elevation.

For instance, when exposed to a 1-W NIR laser, free ICG and CA-1 + ICG experienced temperature elevations of 33 °C and 38.5 °C, respectively, over 10 minutes. A doubling of the laser intensity to 2-W escalated the temperature to 43 °C and 48.5 °C for free ICG and CA-1 + ICG, respectively, in the same time frame. These findings underscore the clear dependence of ICG-loaded hydrogel temperature elevation on NIR laser intensity, a characteristic crucial for inducing hyperthermal effects with the potential to ablate cancer cells [35]. The photothermal conversion efficiency (η) of the ICG-loaded (1 mg/mL) hydrogels irradiated under 808 nm laser (2 $W/cm^{2)}$ for 10 min. was calculated to be 34.6% [85].

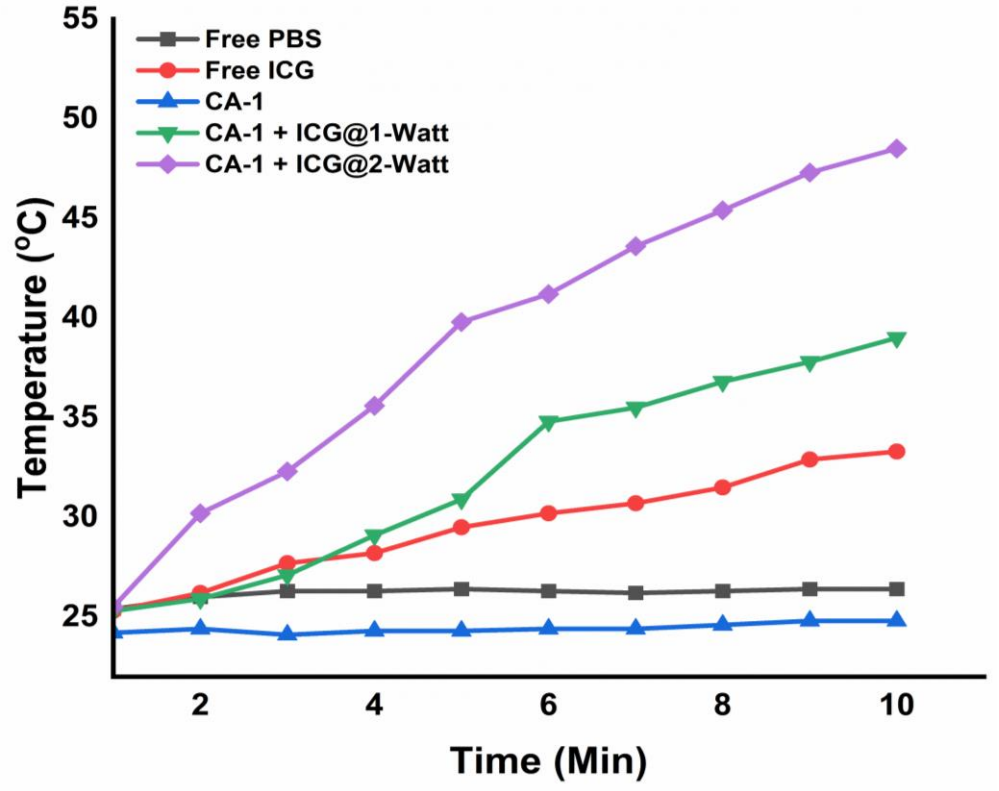

Fig. 30 Photothermal Effect of Free PBS, free ICG, and formulated hydrogels under different intensities of NIR irradiation.

Fig. 31 Photothermal effect of NIR irradiation on hydrogels

3.6.10. Anti-cancer effect of hydrogels.

To investigate the NIR light-induced PDT/PTT and its associated anti-tumor efficacy, CA-1 was suspended in a culture medium containing HeLa cells and subjected to NIR irradiation (2 W, 180 s). The viability of HeLa cells, both with/ without NIR treatment, after incubation with the hydrogels, is graphically represented in Fig. 32. Anti-tumor effect was not significantly observed without NIR irradiation due to absence of ROS and heat generation. By contrast, the high anti-tumor efficacy (i.e, 6% cell viability) of CMC/Alg-derived hydrogels under NIR exposure is indicative of their potential for photothermal and photodynamic therapeutic applications, primarily attributed to the rapid ROS generation and heat within the hydrogel matrix.

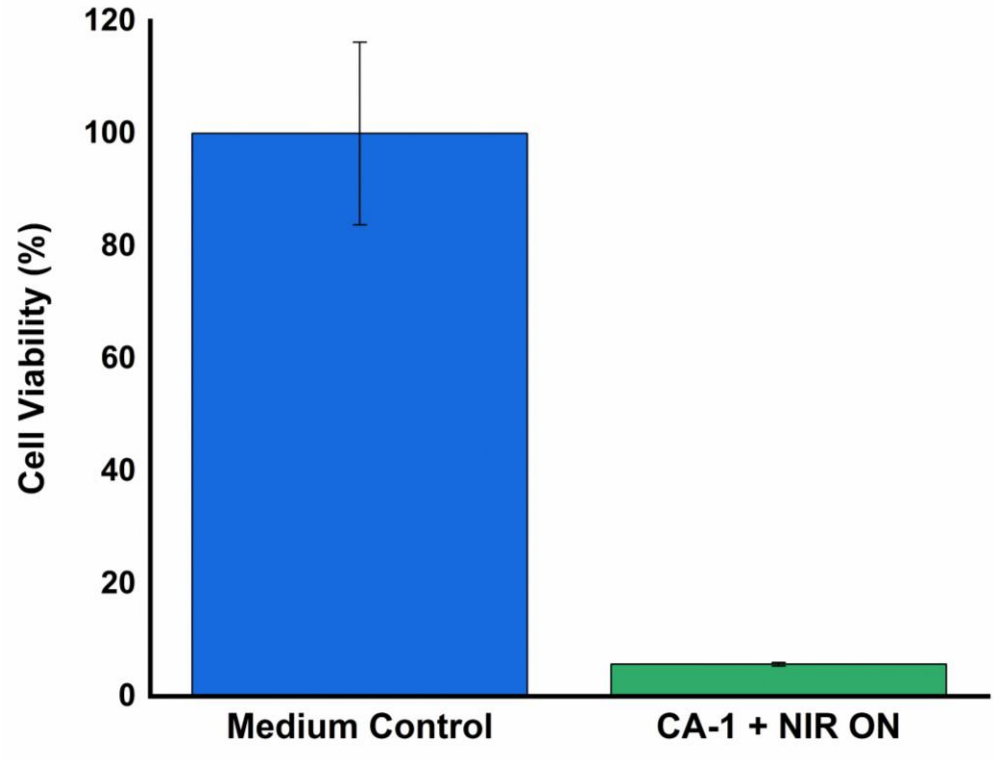

Fig. 32 Anti-cancer treatment against HeLa cancer cells with/without NIR irradiation (2-W power, 180 s)

3.7. Conclusion

The ICG-loaded CMC/Alg hydrogel system was developed for combined PDT and PTT applications. The injectable hydrogels were fabricated through a process of CMC–Alg conjugation, employing CMC functionalized with Nb moieties, which were subsequently reacted with biocompatible Alg modified with mTz through click chemistry. Varying the molar ratio of Alg-mTz within the hydrogel formulations led to distinct mechanical properties, with storage modulus (G') ranging from approximately 492 to 270 Pa. The hydrogels exhibited significant swelling capacity, and high porosity. The hydrogels were examined through DPBF assays to confirm the generation of ROS by NIR light. Upon exposure to different NIR irradiation (1-2 W/cm^2) for prolonged time (5-15 min), the ICG-loaded hydrogel (CA-1) demonstrated a rapid increase in temperature and produced ROS. Cytotoxicity assessments on HEK-293 cells indicated that both precursor materials, CMC–Nb and Alg–mTz, were non-toxic, underscoring their good compatibility with tested cell line. Furthermore, CA-1 hydrogels exhibited notable anti-tumor activity when exposed to NIR radiation, particularly against HeLa cancer cells. Consequently, these hydrogels hold promise for potential applications in combined PTT and PDT.

Chapter 4: Conclusion and Summary

In recent years, there has been a growing recognition of the critical importance of developing drug delivery systems (DDS) that exhibit key features, including on-demand release triggered by non-invasive methods, as well as spatiotemporal control release. This is particularly crucial in the fields of medical treatments, irrespective of the potency of the active therapeutic ingredient. The failure to achieve targeted drug delivery represents a significant challenge in DDS development, posing risks not only to therapeutic efficacy but also potentially inducing adverse effects in normal tissues. Consequently, the utilization of safe and non-invasive stimuli for triggering therapeutic agent is need for an hour. Therefore, the development of DDS employing stimuli-responsive hydrogels assumes paramount significance in overcoming these limitations. Biopolymers, characterized by suitable viscoelastic properties, excellent biocompatibility, favorable swelling properties, rapid degradation profiles, are acknowledged for their potential in this regard. Within this conceptual framework, this dissertation presents two distinct investigations aimed at the design, synthesis, and characterization of stimuli-responsive DDS based on gelatin, CMC/Alg hydrogels, with the objective of assessing their viability for application in cancer therapy.

The whole work can be summarized as follows:

In the first chapter, NIR and reduction-responsive gelatin hydrogels were designed for anti-tumor drug delivery application. Gelatin was functionalized with norbornene (Gel-Nb), followed by covalently cross-linking with a tetrazine (Tz)-based cross-linker (DSe-DPEG-DTz) possessing a redox-cleavable diselenide moiety. The resulting hydrogels were highly porous thanks to the N_2 gas produced during the inverse electron demand Diels Alder ‘‘click reaction’’

between Nb and Tz. The hydrogels exhibited enhanced drug loading efficiency (≈ 94%) and excellent swelling ratios. The hydrogel prepared from the Nb:Tz mol. ratio of 10:10 (GHG-C) showed a storage modulus of 1100 Pa with an elastic rheological property. The doxorubicin (DOX)-loaded hydrogels (AR1) released minimal amounts (26%) of DOX at a physiological condition (PBS, pH 7.4). On the contrary, a fast release of DOX was observed in a reducing environment, where >95% of DOX was released from AR3 after 48 h. The DOX and indocyanine green (ICG) co-loaded hydrogels (AR6) showed a burst release of DOX (>60% after 12 h) upon NIR irradiation, followed by a sustained release of the drug. The combined stimuli of GSH and NIR showed ≈ 85% in half of the total time. Gel-Nb, the cross-linker, and GHG-C were essentially non-toxic to the tested cell lines. Furthermore, AR3 and AR6 restricted the metabolic activities of BT-20 cells after treatment with GSH and NIR irradiation, respectively.

In the second chapter, a novel chemically cross-linked hydrogel was prepared through the utilization of the norbornene (Nb)-methyl tetrazine (mTz) click reaction, derived from carboxymethyl cellulose (CMC) and alginate (Alg). The hydrogel was designed to generate reactive oxygen species (ROS) from NIR-dye, indocyanine green (ICG) for a combined photothermal and photodynamic therapy (PTT/PDT). The cross-linking of Nb and mTz moieties occurred via an inverse electron-demand Diels-Alder reaction under physiological conditions avoiding the need for a catalyst. The resulting hydrogels exhibited viscoelastic properties ($G' \sim 492\text{-}270$ Pa) and high porosity. The hydrogels were found to be injectable with tunable mechanical characteristics. The ICG encapsulated hydrogels demonstrated ROS generation ability under NIR exposure. The ROS production was investigated through DPBF assays to access photodynamic

effect (with NIR irradiation at 1-2W for 5-15 min). The temperature of the ICG-loaded hydrogels was also raised upon the NIR irradiation to eradicate tumor cells photothermally. In vitro cytocompatibility assessments revealed the non-toxic nature of CMC-Nb and Alg-mTz towards HEK-293 cells. Furthermore, the ICG-loaded hydrogels effectively inhibited the metabolic activity of Hela cells following NIR exposure. This innovative hydrogel system holds promise for applications in combined PTT and PDT.

This thesis demonstrated that both Gelatin and CMC/Alg hydrogels can be used as drug carrier together providing internal/external stimuli for anti-tumor applications.

Perspective of Future Work

Throughout the course of this research several areas of interests for further optimization of DDS have been identified as follows:

- Further *in vivo* studies are needed to evaluate the Gelatin-derived hydrogels.
- Adjusting the CMC/Alg hydrogels to obtain best cross-linking density according to the desirable applications and in vivo studies can be further evaluated for anti-tumor application.

List of Publications

- Rizwan, A.; Gulfam, M.; Jo, S.-H.; Seo, J.-W.; Ali, I.; Thang Vu, T.; Joo, S.-B.; Park, S.-H.; Taek Lim, K. Gelatin-based NIR and reduction-responsive injectable hydrogels cross-linked through IEDDA click chemistry for drug delivery application. European Polymer Journal. 2023, 191, 112019, https://doi.org/10.1016/j.eurpolymj.2023.112019.
- Rizwan, A.; Ali, I.; Jo, S.; Vu, T.T.; Gal, Y.; Kim, Y.H.; Park, S.; Lim, K.T. Facile Fabrication of NIR-Responsive Alginate/CMC Hydrogels Derived through IEDDA Click Chemistry for Photothermal-Photodynamic Anti-tumor Therapy. Gels. 2023,9(12), 961, https://doi.org/10.3390/gels9120961.

Bibliography

1. Hoffman, A.S. Hydrogels for biomedical applications. *Advanced Drug Delivery Reviews* **2012**, *64*, 18-23, doi:https://doi.org/10.1016/j.addr.2012.09.010.
2. Lee, K.Y.; Mooney, D.J. Hydrogels for Tissue Engineering. *Chemical Reviews* **2001**, *101*, 1869-1880, doi:10.1021/cr000108x.
3. Thakur, S.; Sharma, B.; Verma, A.; Chaudhary, J.; Tamulevicius, S.; Thakur, V.K. Recent progress in sodium alginate based sustainable hydrogels for environmental applications. *Journal of Cleaner Production* **2018**, *198*, 143-159, doi:https://doi.org/10.1016/j.jclepro.2018.06.259.
4. Li, Z.; Lin, Z. Recent advances in polysaccharide-based hydrogels for synthesis and applications. *Aggregate* **2021**, *2*, e21.
5. Sarwar, M.S.; Ghaffar, A.; Huang, Q.; Khalid, M.; Anwar, A.; Alayoubi, A.M.; Latif, M. Controlled drug release contenders comprising starch/poly(allylamine hydrochloride) biodegradable composite films. *International Journal of Biological Macromolecules* **2023**, *241*, 124598, doi:https://doi.org/10.1016/j.ijbiomac.2023.124598.
6. Yue, S.; He, H.; Li, B.; Hou, T. Hydrogel as a Biomaterial for Bone Tissue Engineering: A Review. *Nanomaterials (Basel)* **2020**, *10*, doi:10.3390/nano10081511.
7. Budiarso, I.J.; Rini, N.D.W.; Tsalsabila, A.; Birowosuto, M.D.; Wibowo, A. Chitosan-Based Smart Biomaterials for Biomedical Applications: Progress and Perspectives. *ACS Biomaterials Science & Engineering* **2023**, *9*, 3084-3115, doi:10.1021/acsbiomaterials.3c00216.
8. Li, Q.; Zhang, S.; Du, R.; Yang, Y.; Liu, Y.; Wan, Z.; Yang, X. Injectable Self-Healing Adhesive Natural Glycyrrhizic Acid Bioactive Hydrogel for Bacteria-Infected Wound Healing. *ACS Applied Materials & Interfaces* **2023**, *15*, 17562-17576, doi:10.1021/acsami.2c23231.
9. Qiu, Y.; Park, K. Environment-sensitive hydrogels for drug delivery. *Advanced Drug Delivery Reviews* **2001**, *53*, 321-339, doi:https://doi.org/10.1016/S0169-409X(01)00203-4.
10. Singh, B.; Sharma, V. Influence of polymer network parameters of tragacanth gum-based pH responsive hydrogels on drug delivery. *Carbohydrate Polymers* **2014**, *101*, 928-940, doi:https://doi.org/10.1016/j.carbpol.2013.10.022.
11. Gao, G.; Jiang, Y.-W.; Jia, H.-R.; Wu, F.-G. Near-infrared light-controllable on-demand antibiotics release using thermo-sensitive

hydrogel-based drug reservoir for combating bacterial infection. *Biomaterials* **2019**, *188*, 83-95, doi:https://doi.org/10.1016/j.biomaterials.2018.09.045.

12. Li, X.; Bian, S.; Zhao, M.; Han, X.; Liang, J.; Wang, K.; Jiang, Q.; Sun, Y.; Fan, Y.; Zhang, X. Stimuli-responsive biphenyl-tripeptide supramolecular hydrogels as biomimetic extracellular matrix scaffolds for cartilage tissue engineering. *Acta Biomaterialia* **2021**, *131*, 128-137, doi:https://doi.org/10.1016/j.actbio.2021.07.007.
13. Naranjo-Alcazar, R.; Bendix, S.; Groth, T.; Gallego Ferrer, G. Research Progress in Enzymatically Cross-Linked Hydrogels as Injectable Systems for Bioprinting and Tissue Engineering. *Gels* **2023**, *9*, 230.
14. Parhi, R. Cross-Linked Hydrogel for Pharmaceutical Applications: A Review. *Adv Pharm Bull* **2017**, *7*, 515-530, doi:10.15171/apb.2017.064.
15. Kharkar, P.M.; Rehmann, M.S.; Skeens, K.M.; Maverakis, E.; Kloxin, A.M. Thiol–ene Click Hydrogels for Therapeutic Delivery. *ACS Biomaterials Science & Engineering* **2016**, *2*, 165-179, doi:10.1021/acsbiomaterials.5b00420.
16. Li, X.; Xiong, Y. Application of "Click" Chemistry in Biomedical Hydrogels. *ACS Omega* **2022**, *7*, 36918-36928, doi:10.1021/acsomega.2c03931.
17. Cadamuro, F.; Russo, L.; Nicotra, F. Biomedical Hydrogels Fabricated Using Diels–Alder Crosslinking. *European Journal of Organic Chemistry* **2021**, *2021*, 374-382, doi:https://doi.org/10.1002/ejoc.202001042.
18. Xu, J.; Liu, Y.; Hsu, S.-h. Hydrogels Based on Schiff Base Linkages for Biomedical Applications. *Molecules* **2019**, *24*, 3005.
19. Dimmitt, N.H.; Arkenberg, M.R.; de Lima Perini, M.M.; Li, J.; Lin, C.-C. Hydrolytically Degradable PEG-Based Inverse Electron Demand Diels–Alder Click Hydrogels. *ACS Biomaterials Science & Engineering* **2022**, *8*, 4262-4273, doi:10.1021/acsbiomaterials.2c00714.
20. Caldorera-Moore, M.; Peppas, N.A. Micro- and nanotechnologies for intelligent and responsive biomaterial-based medical systems. *Adv Drug Deliv Rev* **2009**, *61*, 1391-1401, doi:10.1016/j.addr.2009.09.002.
21. Kim, Y.; Jeong, D.; Shinde, V.V.; Hu, Y.; Kim, C.; Jung, S. Azobenzene-grafted carboxymethyl cellulose hydrogels with photo-switchable, reduction-responsive and self-healing properties for a controlled drug release system. *International Journal of Biological Macromolecules* **2020**, *163*, 824-832, doi:https://doi.org/10.1016/j.ijbiomac.2020.07.071.
22. Lima-Sousa, R.; de Melo-Diogo, D.; Alves, C.G.; Cabral, C.S.D.; Miguel, S.P.; Mendonça, A.G.; Correia, I.J. Injectable in situ forming

thermo-responsive graphene based hydrogels for cancer chemo-photothermal therapy and NIR light-enhanced antibacterial applications. *Materials Science and Engineering: C* **2020**, *117*, 111294, doi:https://doi.org/10.1016/j.msec.2020.111294.

23. Zheng, D.; Bai, B.; Zhao, H.; Xu, X.; Hu, N.; Wang, H. Stimuli-responsive Ca-alginate-based photothermal system with enhanced foliar adhesion for controlled pesticide release. *Colloids and Surfaces B: Biointerfaces* **2021**, *207*, 112004, doi:https://doi.org/10.1016/j.colsurfb.2021.112004.
24. Ding, M.; Jing, L.; Yang, H.; Machnicki, C.E.; Fu, X.; Li, K.; Wong, I.Y.; Chen, P.Y. Multifunctional soft machines based on stimuli-responsive hydrogels: from freestanding hydrogels to smart integrated systems. *Materials Today Advances* **2020**, *8*, 100088, doi:https://doi.org/10.1016/j.mtadv.2020.100088.
25. Shigemitsu, H.; Hamachi, I. Design Strategies of Stimuli-Responsive Supramolecular Hydrogels Relying on Structural Analyses and Cell-Mimicking Approaches. *Accounts of Chemical Research* **2017**, *50*, 740-750, doi:10.1021/acs.accounts.7b00070.
26. Fleige, E.; Quadir, M.A.; Haag, R. Stimuli-responsive polymeric nanocarriers for the controlled transport of active compounds: Concepts and applications. *Advanced Drug Delivery Reviews* **2012**, *64*, 866-884, doi:https://doi.org/10.1016/j.addr.2012.01.020.
27. Tenório-Neto, E.T.; Guilherme, M.R.; Lima-Tenório, M.K.; Scariot, D.B.; Nakamura, C.V.; Rubira, A.F.; Kunita, M.H. Synthesis and characterization of a pH-responsive poly(ethylene glycol)-based hydrogel: acid degradation, equilibrium swelling, and absorption kinetic characteristics. *Colloid and Polymer Science* **2015**, *293*, 3611-3622, doi:10.1007/s00396-015-3744-z.
28. Vu, T.T.; Gulfam, M.; Jo, S.-H.; Park, S.-H.; Lim, K.T. Injectable and biocompatible alginate-derived porous hydrogels cross-linked by IEDDA click chemistry for reduction-responsive drug release application. *Carbohydrate Polymers* **2022**, *278*, 118964, doi:https://doi.org/10.1016/j.carbpol.2021.118964.
29. Marques, A.C.; Costa, P.J.; Velho, S.; Amaral, M.H. Stimuli-responsive hydrogels for intratumoral drug delivery. *Drug Discovery Today* **2021**, *26*, 2397-2405, doi:https://doi.org/10.1016/j.drudis.2021.04.012.
30. Huang, J.; Zhao, L.; Wang, T.; Sun, W.; Tong, Z. NIR-Triggered Rapid Shape Memory PAM–GO–Gelatin Hydrogels with High Mechanical Strength. *ACS Applied Materials & Interfaces* **2016**, *8*, 12384-12392, doi:10.1021/acsami.6b00867.

31. Shi, K.; Liu, Z.; Wei, Y.-Y.; Wang, W.; Ju, X.-J.; Xie, R.; Chu, L.-Y. Near-infrared light-responsive poly (N-isopropylacrylamide)/graphene oxide nanocomposite hydrogels with ultrahigh tensibility. *ACS applied materials & interfaces* **2015**, *7*, 27289-27298.
32. Tang, C.-Y.; Wu, F.-Y.; Yang, M.-K.; Guo, Y.-M.; Lu, G.-H.; Yang, Y.-H. A Classic Near-Infrared Probe Indocyanine Green for Detecting Singlet Oxygen. *International Journal of Molecular Sciences* **2016**, *17*, 219.
33. Kildahl, N.K. Bond Energy Data Summarized. *Journal of Chemical Education* **1995**, *72*, 423, doi:10.1021/ed072p423.
34. Won, H.J.; Ryplida, B.; Kim, S.G.; Lee, G.; Ryu, J.H.; Park, S.Y. Diselenide-Bridged Carbon-Dot-Mediated Self-Healing, Conductive, and Adhesive Wireless Hydrogel Sensors for Label-Free Breast Cancer Detection. *ACS Nano* **2020**, *14*, 8409-8420, doi:10.1021/acsnano.0c02517.
35. Anugrah, D.S.B.; Ramesh, K.; Kim, M.; Hyun, K.; Lim, K.T. Near-infrared light-responsive alginate hydrogels based on diselenide-containing cross-linkage for on demand degradation and drug release. *Carbohydrate Polymers* **2019**, *223*, 115070, doi:https://doi.org/10.1016/j.carbpol.2019.115070.
36. Vandelli, M.A.; Rivasi, F.; Guerra, P.; Forni, F.; Arletti, R. Gelatin microspheres crosslinked with d,l-glyceraldehyde as a potential drug delivery system: preparation, characterisation, in vitro and in vivo studies. *International Journal of Pharmaceutics* **2001**, *215*, 175-184, doi:https://doi.org/10.1016/S0378-5173(00)00681-5.
37. Tabata, Y.; Ikada, Y. Vascularization effect of basic fibroblast growth factor released from gelatin hydrogels with different biodegradabilities. *Biomaterials* **1999**, *20*, 2169-2175, doi:https://doi.org/10.1016/S0142-9612(99)00121-0.
38. Santoro, M.; Tatara, A.M.; Mikos, A.G. Gelatin carriers for drug and cell delivery in tissue engineering. *Journal of Controlled Release* **2014**, *190*, 210-218, doi:https://doi.org/10.1016/j.jconrel.2014.04.014.
39. Bello, A.B.; Kim, D.; Kim, D.; Park, H.; Lee, S.H. Engineering and Functionalization of Gelatin Biomaterials: From Cell Culture to Medical Applications. *Tissue engineering. Part B, Reviews* **2020**, *26*, 164-180, doi:10.1089/ten.TEB.2019.0256.
40. Zhang, Y.; Wang, Q.; Wang, Z.; Zhang, D.; Gu, J.; Ye, K.; Su, D.; Zhang, Y.; Chen, J.; Barboiu, M. Strong, Self-Healing Gelatin Hydrogels Cross-Linked by Double Dynamic Covalent Chemistry. *ChemPlusChem* **2021**, *86*, 1524-1529, doi:https://doi.org/10.1002/cplu.202100474.

41. Xu, K.; Cantu, D.A.; Fu, Y.; Kim, J.; Zheng, X.; Hematti, P.; Kao, W.J. Thiol-ene Michael-type formation of gelatin/poly(ethylene glycol) biomatrices for three-dimensional mesenchymal stromal/stem cell administration to cutaneous wounds. *Acta Biomaterialia* **2013**, *9*, 8802-8814, doi:https://doi.org/10.1016/j.actbio.2013.06.021.
42. Jiang, Y.; Chen, J.; Deng, C.; Suuronen, E.J.; Zhong, Z. Click hydrogels, microgels and nanogels: Emerging platforms for drug delivery and tissue engineering. *Biomaterials* **2014**, *35*, 4969-4985, doi:https://doi.org/10.1016/j.biomaterials.2014.03.001.
43. Mũnoz, Z.; Shih, H.; Lin, C.-C. Gelatin hydrogels formed by orthogonal thiol–norbornene photochemistry for cell encapsulation. *Biomaterials Science* **2014**, *2*, 1063-1072, doi:10.1039/C4BM00070F.
44. Siboro, S.A.P.; Anugrah, D.S.B.; Ramesh, K.; Park, S.-H.; Kim, H.-R.; Lim, K.T. Tunable porosity of covalently crosslinked alginate-based hydrogels and its significance in drug release behavior. *Carbohydrate Polymers* **2021**, *260*, 117779, doi:https://doi.org/10.1016/j.carbpol.2021.117779.
45. Gulfam, M.; Jo, S.-H.; Jo, S.-W.; Vu, T.T.; Park, S.-H.; Lim, K.T. Highly porous and injectable hydrogels derived from cartilage acellularized matrix exhibit reduction and NIR light dual-responsive drug release properties for application in antitumor therapy. *NPG Asia Materials* **2022**, *14*, 8, doi:10.1038/s41427-021-00354-4.
46. Van Hoorick, J.; Dobos, A.; Markovic, M.; Gheysens, T.; Van Damme, L.; Gruber, P.; Tytgat, L.; Van Erps, J.; Thienpont, H.; Dubruel, P.; et al. Thiol-norbornene gelatin hydrogels: influence of thiolated crosslinker on network properties and high definition 3D printing. *Biofabrication* **2021**, *13*, 015017, doi:10.1088/1758-5090/abc95f.
47. Zatorski, J.M.; Montalbine, A.N.; Ortiz-Cárdenas, J.E.; Pompano, R.R. Quantification of fractional and absolute functionalization of gelatin hydrogels by optimized ninhydrin assay and (1)H NMR. **2020**, *412*, 6211-6220, doi:10.1007/s00216-020-02792-5.
48. Grover, C.N.; Gwynne, J.H.; Pugh, N.; Hamaia, S.; Farndale, R.W.; Best, S.M.; Cameron, R.E. Crosslinking and composition influence the surface properties, mechanical stiffness and cell reactivity of collagen-based films. *Acta Biomaterialia* **2012**, *8*, 3080-3090, doi:https://doi.org/10.1016/j.actbio.2012.05.006.
49. Bakaic, E.; Smeets, N.M.B.; Hoare, T. Injectable hydrogels based on poly(ethylene glycol) and derivatives as functional biomaterials. *RSC Advances* **2015**, *5*, 35469-35486, doi:10.1039/C4RA13581D.

50. Samanta, H.S.; Ray, S.K. Effect of polyethylene glycol and nano clay on swelling, diffusion, network parameters and drug release behavior of interpenetrating network copolymer. *Journal of Applied Polymer Science* **2022**, *139*, 51678, doi:https://doi.org/10.1002/app.51678.
51. Tanuma, H.; Saito, T.; Nishikawa, K.; Dong, T.; Yazawa, K.; Inoue, Y. Preparation and characterization of PEG-cross-linked chitosan hydrogel films with controllable swelling and enzymatic degradation behavior. *Carbohydrate Polymers* **2010**, *80*, 260-265.
52. Jaiswal, S.; Dutta, S.B.; Nayak, D.; Gupta, S. Effect of Doxorubicin on the Near-Infrared Optical Properties of Indocyanine Green. *ACS Omega* **2021**, *6*, 34842-34849, doi:10.1021/acsomega.1c05500.
53. Panja, A.; Das, S.; Chakraborty, A.; Chakraborty, P.; Pal, S.; Nandi, A.K. Injectable Hydrogel of Vitamin B9 for the Controlled Release of Both Hydrophilic and Hydrophobic Anticancer Drugs. *ChemMedChem* **2018**, *13*, 2427-2436.
54. Von Burkersroda, F.; Schedl, L.; Göpferich, A. Why degradable polymers undergo surface erosion or bulk erosion. *Biomaterials* **2002**, *23*, 4221-4231.
55. Costa, P.; Lobo, J.M.S. Modeling and comparison of dissolution profiles. *European journal of pharmaceutical sciences* **2001**, *13*, 123-133.
56. Dinh, T.N.; Hou, S.; Park, S.; Shalek, B.A.; Jeong, K.J. Gelatin Hydrogel Combined with Polydopamine Coating To Enhance Tissue Integration of Medical Implants. *ACS Biomaterials Science & Engineering* **2018**, *4*, 3471-3477, doi:10.1021/acsbiomaterials.8b00886.
57. Tadsen, M.; Friedrich, R.P.; Riedel, S.; Alexiou, C.; Mayr, S.G. Contact Guidance by Microstructured Gelatin Hydrogels for Prospective Tissue Engineering Applications. *ACS Applied Materials & Interfaces* **2019**, *11*, 7450-7458, doi:10.1021/acsami.8b21638.
58. Conrad, B.; Hayashi, C.; Yang, F. Gelatin-Based Microribbon Hydrogels Support Robust MSC Osteogenesis across a Broad Range of Stiffness. *ACS Biomaterials Science & Engineering* **2020**, *6*, 3454-3463, doi:10.1021/acsbiomaterials.9b01792.
59. Kharkar, P.M.; Kiick, K.L.; Kloxin, A.M. Designing degradable hydrogels for orthogonal control of cell microenvironments. *Chemical Society Reviews* **2013**, *42*, 7335-7372.
60. Ali, I.; Gulfam, M.; Jo, S.-H.; Seo, J.-W.; Rizwan, A.; Park, S.-H.; Lim, K.T. Reduction-responsive and bioorthogonal carboxymethyl cellulose based soft hydrogels cross-linked via IEDDA click chemistry for cancer therapy application. *International Journal of Biological Macromolecules* **2022**, *219*, 109-120.

61. Zhang, C.; Ma, J.; Wang, Q.; Wang, Y.; Kang, Z.; Chen, Y.; Hui, Z.; Wang, X. pH/Thermal Dual-Sensitive Nanoparticle-Hydrogel Composite Based on Pluronic and Carboxymethyl Chitosan for In Situ Injection and Enhanced Chemo-Photothermal Antitumor Effect. *ACS Applied Nano Materials* **2023**, *6*, 7841-7854, doi:10.1021/acsanm.3c00983.
62. Hu, H.; Li, Y.; Zhou, Q.; Ao, Y.; Yu, C.; Wan, Y.; Xu, H.; Li, Z.; Yang, X. Redox-Sensitive Hydroxyethyl Starch–Doxorubicin Conjugate for Tumor Targeted Drug Delivery. *ACS Applied Materials & Interfaces* **2016**, *8*, 30833-30844, doi:10.1021/acsami.6b11932.
63. Hoang, H.T.; Vu, T.T.; Karthika, V.; Jo, S.-H.; Jo, Y.-J.; Seo, J.-W.; Oh, C.-W.; Park, S.-H.; Lim, K.T. Dual cross-linked chitosan/alginate hydrogels prepared by Nb-Tz 'click' reaction for pH responsive drug delivery. *Carbohydrate Polymers* **2022**, *288*, 119389, doi:https://doi.org/10.1016/j.carbpol.2022.119389.
64. Cappetta, D.; Rossi, F.; Piegari, E.; Quaini, F.; Berrino, L.; Urbanek, K.; De Angelis, A. Doxorubicin targets multiple players: A new view of an old problem. *Pharmacol Res* **2018**, *127*, 4-14, doi:10.1016/j.phrs.2017.03.016.
65. Zou, Y.; Li, M.; Xiong, T.; Zhao, X.; Du, J.; Fan, J.; Peng, X. A single molecule drug targeting photosensitizer for enhanced breast cancer photothermal therapy. *Small* **2020**, *16*, 1907677.
66. Jia, Y.P.; Shi, K.; Yang, F.; Liao, J.F.; Han, R.X.; Yuan, L.P.; Hao, Y.; Pan, M.; Xiao, Y.; Qian, Z.Y.; et al. Multifunctional Nanoparticle Loaded Injectable Thermoresponsive Hydrogel as NIR Controlled Release Platform for Local Photothermal Immunotherapy to Prevent Breast Cancer Postoperative Recurrence and Metastases. *Advanced Functional Materials* **2020**, *30*, 2001059, doi:https://doi.org/10.1002/adfm.202001059.
67. Zhang, R.; Yu, B.; Tian, Y.; Pang, L.; Xu, T.; Cong, H.; Shen, Y. Diversified antibacterial modification and latest applications of polysaccharide-based hydrogels for wound healthcare. *Applied Materials Today* **2022**, *26*, 101396, doi:https://doi.org/10.1016/j.apmt.2022.101396.
68. Zhu, T.; Mao, J.; Cheng, Y.; Liu, H.; Lv, L.; Ge, M.; Li, S.; Huang, J.; Chen, Z.; Li, H.; et al. Recent Progress of Polysaccharide-Based Hydrogel Interfaces for Wound Healing and Tissue Engineering. *Advanced Materials Interfaces* **2019**, *6*, 1900761, doi:https://doi.org/10.1002/admi.201900761.

69. Matricardi, P.; Di Meo, C.; Coviello, T.; Hennink, W.E.; Alhaique, F. Interpenetrating Polymer Networks polysaccharide hydrogels for drug delivery and tissue engineering. *Advanced Drug Delivery Reviews* **2013**, *65*, 1172-1187, doi:https://doi.org/10.1016/j.addr.2013.04.002.
70. Radhakrishnan, J.; Subramanian, A.; Krishnan, U.M.; Sethuraman, S. Injectable and 3D bioprinted polysaccharide hydrogels: from cartilage to osteochondral tissue engineering. *Biomacromolecules* **2017**, *18*, 1-26.
71. Carvalho, S.M.; Mansur, A.A.P.; Capanema, N.S.V.; Carvalho, I.C.; Chagas, P.; de Oliveira, L.C.A.; Mansur, H.S. Synthesis and in vitro assessment of anticancer hydrogels composed by carboxymethylcellulose-doxorubicin as potential transdermal delivery systems for treatment of skin cancer. *Journal of Molecular Liquids* **2018**, *266*, 425-440, doi:https://doi.org/10.1016/j.molliq.2018.06.085.
72. Ali, I.; Gulfam, M.; Jo, S.H.; Seo, J.W.; Rizwan, A.; Park, S.H.; Lim, K.T. Reduction-responsive and bioorthogonal carboxymethyl cellulose based soft hydrogels cross-linked via IEDDA click chemistry for cancer therapy application. *Int J Biol Macromol* **2022**, *219*, 109-120, doi:10.1016/j.ijbiomac.2022.07.229.
73. Li, S.; Wang, X.; Chen, J.; Guo, J.; Yuan, M.; Wan, G.; Yan, C.; Li, W.; Machens, H.G.; Rinkevich, Y.; et al. Calcium ion cross-linked sodium alginate hydrogels containing deferoxamine and copper nanoparticles for diabetic wound healing. *Int J Biol Macromol* **2022**, *202*, 657-670, doi:10.1016/j.ijbiomac.2022.01.080.
74. Massana Roquero, D.; Othman, A.; Melman, A.; Katz, E. Iron(iii)-cross-linked alginate hydrogels: a critical review. *Materials Advances* **2022**, *3*, 1849-1873, doi:10.1039/D1MA00959A.
75. Meng, L.; Shao, C.; Yang, J. Ionically cross-linked silk microfibers/alginate tough composite hydrogels with hierarchical structures. *ACS Sustainable Chemistry & Engineering* **2018**, *6*, 16788-16796.
76. Ooi, H.W.; Mota, C.; ten Cate, A.T.; Calore, A.; Moroni, L.; Baker, M.B. Thiol–Ene Alginate Hydrogels as Versatile Bioinks for Bioprinting. *Biomacromolecules* **2018**, *19*, 3390-3400, doi:10.1021/acs.biomac.8b00696.
77. Deng, Y.; Shavandi, A.; Okoro, O.V.; Nie, L. Alginate modification via click chemistry for biomedical applications. *Carbohydrate Polymers* **2021**, *270*, 118360, doi:https://doi.org/10.1016/j.carbpol.2021.118360.
78. Möller, L.; Krause, A.; Dahlmann, J.; Gruh, I.; Kirschning, A.; Dräger, G. Preparation and evaluation of hydrogel-composites from methacrylated hyaluronic acid, alginate, and gelatin for tissue

engineering. *Int J Artif Organs* **2011**, *34*, 93-102, doi:10.5301/ijao.2011.6397.
79. Augé, A.; Camerel, F.; Benoist, A.; Zhao, Y. Near-infrared light-responsive UCST-nanogels using an efficient nickel-bis(dithiolene) photothermal crosslinker. *Polymer Chemistry* **2020**, *11*, 3863-3875, doi:10.1039/D0PY00567C.
80. Jo, Y.-J.; Gulfam, M.; Jo, S.-H.; Gal, Y.-S.; Oh, C.-W.; Park, S.-H.; Lim, K.T. Multi-stimuli responsive hydrogels derived from hyaluronic acid for cancer therapy application. *Carbohydrate Polymers* **2022**, *286*, 119303, doi:https://doi.org/10.1016/j.carbpol.2022.119303.
81. Rizwan, A.; Gulfam, M.; Jo, S.-H.; Seo, J.-W.; Ali, I.; Thang Vu, T.; Joo, S.-B.; Park, S.-H.; Taek Lim, K. Gelatin-based NIR and reduction-responsive injectable hydrogels cross-linked through IEDDA click chemistry for drug delivery application. *European Polymer Journal* **2023**, *191*, 112019, doi:https://doi.org/10.1016/j.eurpolymj.2023.112019.
82. Deng, K.; Hou, Z.; Deng, X.; Yang, P.; Li, C.; Lin, J. Enhanced Antitumor Efficacy by 808 nm Laser-Induced Synergistic Photothermal and Photodynamic Therapy Based on a Indocyanine-Green-Attached W18O49 Nanostructure. *Advanced Functional Materials* **2015**, *25*, 7280-7290, doi:https://doi.org/10.1002/adfm.201503046.
83. Pan, H.; Zhang, C.; Wang, T.; Chen, J.; Sun, S.-K. In Situ Fabrication of Intelligent Photothermal Indocyanine Green–Alginate Hydrogel for Localized Tumor Ablation. *ACS Applied Materials & Interfaces* **2019**, *11*, 2782-2789, doi:10.1021/acsami.8b16517.
84. Desai, R.M.; Koshy, S.T.; Hilderbrand, S.A.; Mooney, D.J.; Joshi, N.S. Versatile click alginate hydrogels crosslinked via tetrazine–norbornene chemistry. *Biomaterials* **2015**, *50*, 30-37, doi:https://doi.org/10.1016/j.biomaterials.2015.01.048.
85. Qi, D.; Zhu, H.; Kong, Y.; Shen, Q. Injectable Nanomedicine–Hydrogel for NIR Light Photothermal–Chemo Combination Therapy of Tumor. *Polymers* **2022**, *14*, 5547.
86. Park, K.; Park, S.S.; Yun, Y.H.; Ha, C.-S. Mesoporous silica nanoparticles functionalized with a redox-responsive biopolymer. *Journal of Porous Materials* **2017**, *24*, 1215-1225, doi:10.1007/s10934-017-0361-x.
87. Ravikrishnan, A.; Zhang, H.; Fox, J.M.; Jia, X. Core–Shell Microfibers via Bioorthogonal Layer-by-Layer Assembly. *ACS Macro Letters* **2020**, *9*, 1369-1375, doi:10.1021/acsmacrolett.0c00515.

88. van Dijk, M.; Rijkers, D.T.S.; Liskamp, R.M.J.; van Nostrum, C.F.; Hennink, W.E. Synthesis and Applications of Biomedical and Pharmaceutical Polymers via Click Chemistry Methodologies. *Bioconjugate Chemistry* **2009**, *20*, 2001-2016, doi:10.1021/bc900087a.
89. Saxena, A.; Kaloti, M.; Bohidar, H.B. Rheological properties of binary and ternary protein-polysaccharide co-hydrogels and comparative release kinetics of salbutamol sulphate from their matrices. *Int J Biol Macromol* **2011**, *48*, 263-270, doi:10.1016/j.ijbiomac.2010.11.008.
90. Gulfam, M.; Jo, S.-H.; Vu, T.T.; Ali, I.; Rizwan, A.; Joo, S.-B.; Park, S.-H.; Lim, K.T. NIR-degradable and biocompatible hydrogels derived from hyaluronic acid and coumarin for drug delivery and bio-imaging. *Carbohydrate Polymers* **2023**, *303*, 120457, doi:https://doi.org/10.1016/j.carbpol.2022.120457.
91. Han, J.; Lei, T.; Wu, Q. High-water-content mouldable polyvinyl alcohol-borax hydrogels reinforced by well-dispersed cellulose nanoparticles: Dynamic rheological properties and hydrogel formation mechanism. *Carbohydrate Polymers* **2014**, *102*, 306-316, doi:https://doi.org/10.1016/j.carbpol.2013.11.045.
92. Li, X.; Du, X.; Gao, Y.; Shi, J.; Kuang, Y.; Xu, B. Supramolecular hydrogels formed by the conjugates of nucleobases, Arg-Gly-Asp (RGD) peptides, and glucosamine. *Soft Matter* **2012**, *8*, 7402-7407, doi:10.1039/C2SM25725D.
93. Yan, C.; Pochan, D.J. Rheological properties of peptide-based hydrogels for biomedical and other applications. *Chemical Society Reviews* **2010**, *39*, 3528-3540, doi:10.1039/B919449P.
94. Jeong, D.; Joo, S.-W.; Hu, Y.; Shinde, V.V.; Cho, E.; Jung, S. Carboxymethyl cellulose-based superabsorbent hydrogels containing carboxymehtyl β-cyclodextrin for enhanced mechanical strength and effective drug delivery. *European Polymer Journal* **2018**, *105*, 17-25, doi:https://doi.org/10.1016/j.eurpolymj.2018.05.023.
95. Chen, T.; Yao, T.; Peng, H.; Whittaker, A.K.; Li, Y.; Zhu, S.; Wang, Z. An Injectable Hydrogel for Simultaneous Photothermal Therapy and Photodynamic Therapy with Ultrahigh Efficiency Based on Carbon Dots and Modified Cellulose Nanocrystals. *Advanced Functional Materials* **2021**, *31*, 2106079, doi:https://doi.org/10.1002/adfm.202106079.